# DEDUCING TURBULENCE PARAMETERS FROM TRANSIONOSPHERIC SCINTILLATION MEASUREMENTS

A. BHATTACHARYYA

*Indian Institute of Geomagnetism, Bombay, India*

K. C. YEH and S. J. FRANKE

*Wave Propagation Laboratory, Department of Electrical and Computer Engineering, University of Illinois, Urbana, IL 61801, U.S.A.*

(Received 7 February, 1991; accepted 11 February, 1992)

**Abstract.** The theoretical framework and experimental methodology used to interpret observations of ionospheric scintillations in terms of geophysical processes are reviewed and recent experimental observations of ionospheric scintillations are discussed in this paper. During the past 15 years significant progress has been made in several areas. In particular, significant advances have been made in theoretical understanding of the strong scintillation regime and the effects of short-term temporal variations of the scintillation producing irregularities on observations made with spaced-receiver geometries in both weak and strong scintillations. This improved understanding of the scintillation process has significantly increased the utility of the technique particularly in the equatorial latitudes where geometrical effects are least important.

## 1. Introduction

Over last few decades, use of ionospheric scintillation observations to monitor density irregularities present in ionospheric plasma has become widespread. This has happened because, apart from their direct impact on problems related to transionospheric communication, measurements of ionospheric scintillation can be utilized to deduce certain characteristics of ionospheric density fluctuations which give riese to the scintillations. The scintillations or fluctuations in amplitude and phase of a radio wave emitted from a source beyond the ionosphere are recorded by receivers on the ground. The source may be a radio star, an orbiting or a geostationary satellite. Scintillations have been observed on signals covering a wide range of frequencies extending from HF to gigahertz frequencies.

A comprehensive theoretical framework for describing ionospheric scintillations now exists, and this is utilized to extract information about ionospheric turbulence from scintillation data. In the earliest theories, the effect of irregularities on a radio wave traversing through them was considered in terms of a phase changing screen placed in the path of the wave (Booker *et al.*, 1950; Hewish, 1951; Bramley, 1954; Ratcliffe, 1956). The possibility of a phase screen imposing large phase fluctuations on a radio wave was also considered (Mercier, 1962). Later, effects of the finite thickness of the irregularity layer were introduced in the theory for the case of weak scintillations (Barabenenkov *et al.*, 1971). In recent years, in endeavors to explain observed features of strong scintillations, the emphasis has been on finding solutions of equations satisfied by moments of the wave field (Yeh *et al.*, 1975; Booker *et al.*, 1985; Kumagai, 1987;

*Space Science Reviews* **61:** 335–386, 1992.

Bhattacharyya and Yeh, 1988). Another approach that has proved to be useful is that of computer simulations of radio wave propagation through ionospheric irregularities (Franke and Liu, 1983). Many of these theoretical developments have been discussed in detail in a review paper by Yeh and Liu (1982).

In earlier work on scintillations, it was assumed that the ionospheric irregularities are 'frozen', i.e., they are only spatial variations in the electron density which convect with a uniform velocity, without any change in their spatial structures. In that situation, temporal fluctuations of amplitude and phase of a radio wave recorded by a receiver are solely due to movement of the diffraction pattern on the ground. This motion is brought about by either convection of the irregularities across the path of the signal from a geostationary satellite to the receiver, or, in the case of an orbiting satellite, due to the motion of the source itself which is much faster than that of the irregularities so that the signal path essentially scans over the spatial variations in the irregular medium. The assumption of 'frozen' irregularities was found to be adequate for single receiver observations of scintillations. However, 'non-frozen' effects due to temporal variation of irregularities became evident in spaced receiver measurements of scintillation (Wernik *et al.*, 1983) which provided additional information about the behavior of irregularities. Proper interpretation of spaced-receiver measurements called for theoretical investigation of the relationship of space-time characteristics of scintillations and the pattern of space-time variations of ionospheric irregularities (Wernik *et al.*, 1983; Franke, 1987; Bhattacharyya *et al.*, 1989).

There are basically two different approaches to the study of ionospheric scintillations. One is based on a deterministic picture of the ionospheric irregularities. Given the complex nature of the irregularities, which generally result from nonlinear evolution of certain plasma instabilities in the ionosphere, this description is usually very complicated and only amenable to computer simulation studies. The other approach is based on a stochastic description where the space-time variations in density, which constitute the irregularities, are characterized by their statistical properties. Theories of wave propagation in random media are used to relate irregularity characteristics with certain statistical parameters of the resultant amplitude and phase scintillations, such as their power spectra, which can be derived from observations. It is not possible to determine some features of the irregularity layer such as its height, thickness and mean-square electron density fluctuation, uniquely from scintillation observations. However, supplementary information obtained from *in situ* measurements using rockets or satellites, and from radar observations, are often utilized in deducing ionospheric turbulence parameters from scintillation data.

Features of ionospheric irregularities obtained from scintillation data collected in different geographic regions show characteristic differences. These disparities arise because plasma processes responsible for the generation of irregularities usually differ from one region to another, depending on ambient conditions prevalent there in terms of density gradients, electric fields, drift of electrons relative to ions, collision frequencies, geometry of the geomagnetic field, etc. An example of this is the difference between the geometry of the geomagnetic field, which plays an important role in certain

plasma instabilities, in the equatorial and auroral ionospheres. A number of ionospheric parameters which play a role in the generation and sustenance of ionospheric irregularities (Fejer and Kelley, 1980) are controlled by local time and season. The level of geomagnetic activity and solar activity are other factors which affect these parameters. Some of these effects on the characteristics of ionospheric irregularities have been studied using scintillation observations. Interpretation of the results in terms of geophysical phenomena contributes towards a better understanding of the plasma processes occurring in, and electrodynamics of, the upper atmosphere.

## 2. Theories of Scintillation

### 2.1. Statistical characterization in the medium

In the theories of scintillation, ionospheric irregularities are usually described as a random medium with certain statistical properties. The electron density fluctuations, which constitute the irregularities, in general not only move across the path of the radio wave in its transit through the ionosphere, but also change with time because there is evolution or decay of plasma instabilities due to diffusion or other causes. Therefore, at any point of the irregularity layer, deviation $\Delta N$ of electron density, from its average value, is a function of the coordinates of that point as well as time. This implies a space-time dependent refractive index for the layer. Phase variation imposed on a plane wave propagating along the $z$-axis, by fluctuations $\Delta n$ in the ionospheric refractive index is given by

$$\phi(\boldsymbol{\rho}, t) = \frac{2\pi}{\lambda} \int \Delta n(\boldsymbol{\rho}, z, t)\, \mathrm{d}z\,, \tag{2.1}$$

where $\lambda$ is the signal wavelength. There is obviously negligible change in the refractive index during the time interval required for the signal to travel through the irregularity layer. In terms of the deviation $\Delta N_T$ in the total electron content along the path of the wave, the phase change is given by

$$\phi(\boldsymbol{\rho}, t) = -\lambda r_e \Delta N_T(\boldsymbol{\rho}, t)\,, \tag{2.2}$$

where

$$\Delta N_T(\boldsymbol{\rho}, t) = \int \Delta N(\boldsymbol{\rho}, z, t)\, \mathrm{d}z \tag{2.3}$$

and $r_e$ ($= e^2/4\pi m \varepsilon_0 c^2$) is the classical electron radius.

Space-time correlation function of the phase perturbation given in (2.2) is determined by the space-time correlation function $B_{\Delta N_T}(\boldsymbol{\rho}, t)$ of $\Delta N_T$ which is defined by

$$B_{\Delta N_T}(\boldsymbol{\rho}, t) = \langle \Delta N_T(\boldsymbol{\rho} + \boldsymbol{\rho}', t + t') \Delta N_T(\boldsymbol{\rho}', t') \rangle\,, \tag{2.4}$$

where angular brackets represent an ensemble average. In most cases the irregularity

layer thickness is large compared to the correlation length of the electron density irregularities along the $z$-direction. Then $B_{\Delta N_T}$ can be approximated by

$$B_{\Delta N_T}(\boldsymbol{\rho}, t) \simeq L \int_{-\infty}^{\infty} B_{\Delta N}(\boldsymbol{\rho}, z, t)\, \mathrm{d}z\,, \tag{2.5}$$

where $L$ is the path length of the wave inside the irregular medium. The integrated correlation function $A_{\Delta N}(\boldsymbol{\rho}, t)$ defined as

$$A_{\Delta N}(\boldsymbol{\rho}, t) = \int_{-\infty}^{\infty} B_{\Delta N}(\boldsymbol{\rho}, z, t)\, \mathrm{d}z \tag{2.6}$$

represents the effect of the irregularities on the incident wave. It can be expressed in terms of the space-time power spectrum $S_{\Delta N}(\mathbf{k}, \omega)$ of the irregularities which is the Fourier transform of the correlation function $B_{\Delta N}(\mathbf{r}, t)$

$$A_{\Delta N}(\boldsymbol{\rho}, t) = 2\pi \int\int_{-\infty}^{\infty} S_{\Delta N}(\mathbf{k}_\perp, k_z = 0, t)\, e^{+i\mathbf{k}_\perp \cdot \boldsymbol{\rho}}\, \mathrm{d}\mathbf{k}_\perp\,, \tag{2.7}$$

where

$$S_{\Delta N}(\mathbf{k}, \omega) = (2\pi)^{-4} \int\int\int\int B_{\Delta N}(\mathbf{r}, t)\, e^{-i(\mathbf{k}\cdot\mathbf{r} + \omega t)}\, \mathrm{d}\mathbf{r}\, \mathrm{d}t\,. \tag{2.8}$$

In the scattering of electromagnetic waves by a turbulent plasma, this frequency dependent spectrum plays a role where the returned signal shows both a Doppler shift and frequency broadening. There are two processes at work here: (a) temporal variation of the scattering eddies in a coordinate system which moves with the local velocity; (b) movement of the irregularities as a whole with an average velocity. Recognizing this, Shkarofsky (1968) assumed that the characteristic scale lengths required for a representation of the spectrum are independent of time. There may be two such scale lengths in the system, characterizing, respectively, irregularity scale sizes which contain maximum energy and those which undergo rapid dissipation. With the above assumption, Shkarofsky (1968) decomposed $S_{\Delta N}(\mathbf{k}, \omega)$ as follows

$$S_{\Delta N}(\mathbf{k}, \omega) = \Phi_{\Delta N}(\mathbf{k})\, \Psi(\mathbf{k}, \omega)\,, \tag{2.9}$$

where $\Psi(\mathbf{k}, \omega)$ is normalized to unity

$$\int \Psi(\mathbf{k}, \omega)\, \mathrm{d}\omega = 1 \tag{2.10}$$

and $\Phi_{\Delta N}(\mathbf{k})$ is the power spectrum of 'frozen' irregularities. The function $\Psi(\mathbf{k}, \omega)$, or its temporal Fourier transform $\Psi(\mathbf{k}, t)$, is associated with various decay mechanisms such as diffusion or velocity fluctuations, in the case of 'non-frozen' irregularities. For 'frozen' irregularities which simply convect with a uniform velocity $\mathbf{V}_0$ without changing

their spatial structure,

$$\Delta N(\mathbf{r}, t + t') = \Delta N(\mathbf{r} - \mathbf{V}_0 t, t') , \tag{2.11}$$

which yields

$$B_{\Delta N}(\mathbf{r}, t) = B_{\Delta N}(\mathbf{r} - \mathbf{V}_0 t) . \tag{2.12}$$

Therefore, in this case,

$$S_{\Delta N}(\mathbf{k}, \omega) = \Phi_{\Delta N}(\mathbf{k}) \delta(\mathbf{k} \cdot \mathbf{V}_0 + \omega) . \tag{2.13}$$

*In situ* measurements of ionospheric density fluctuations have been made by probes on rockets and satellites (Dyson *et al.*, 1974; Basu *et al.*, 1980, 1983; Rino *et al.*, 1981). From these data, a one-dimensional spectrum is obtained which corresponds to the spatial variations measured in the direction of motion of the probe. The movement of a satellite or a rocket is rapid enough that temporal changes in the irregularities do not come into the picture. If it is assumed that the density irregularities are isotropic, a one-dimensional spectrum can be related to the three-dimensional spectrum in a straightforward manner (Yeh and Liu, 1982). Early *in situ* measurements of the spectral characteristics of *F*-region ionospheric irregularities (Dyson, 1974; Fejer and Kelley, 1980) yielded a one-dimensional spectrum of the power law form: $\Phi_{\Delta N}(k_x) \propto k_x^{-m}$ with $m \approx 2$ for a range of irregularity scale-sizes extending from about 100 m to 10 km. With the assumption of isotropic irregularities, the corresponding three-dimensional spectrum would have the power-law form: $\Phi_{\Delta N}(\mathbf{k}) \propto k^{-4}$. Since different physical processes are responsible for the growth and sustenance of ionospheric density irregularities in different scale size regimes, it is expected that a given power-law form of the density spectrum will be applicable only within an inner and outer scale. For instance, a measured one-dimensional irregularity power spectrum may sometimes exhibit two or more power-law regimes with different spectral indices (Rino *et al.*, 1981; Basu *et al.*, 1983; Singh and Szuszczewicz, 1984; LaBelle and Kelley, 1986). These observational results have, in some cases, been incorporated in theoretical modeling of ionospheric irregularities for the interpretation of scintillation observations.

## 2.2. Phase screen approximation

The earliest theories of ionospheric scintillation were based on the phase screen approximation according to which the irregularities are confined to a single screen of infinitesimal thickness. When a plane wave, propagating along the $z$-direction, traverses this screen, which is assumed to be located in the plane $z = 0$, phase fluctuations given by (2.2) are imposed on it. Components of the electric field associated with this wave are usually expressed in terms of a space-time dependent complex amplitude $u(\mathbf{r}, t)$, which has a value of unity for an incident wave of unit amplitude before it enters the irregularity layer

$$E(\mathbf{r}, t) = u(\mathbf{r}, t) e^{-ikz} , \tag{2.14}$$

where $k = 2\pi/\lambda$ is the signal wave number. Immediately after the wave emerges from

the phase screen, its complex amplitude is given by

$$u(\mathbf{r}, t) = \exp[-i\phi(\boldsymbol{\rho}, t)] \tag{2.15}$$

because of the imposed phase perturbation. Diffraction pattern of the wave in the region beyond the phase screen can now be obtained using Kirchoff's formula (Ratcliffe, 1956), which gives the scalar wave field in this region as an integral of the wave field given by (2.15) and its spatial derivative. It is assumed that the typical scale size of irregularities which play a dominant role in causing scintillations is much greater than the signal wavelength. Further, this characteristic scale size is assumed to be much smaller than the distance the wave travels from the phase screen to the receiver, so that the wave is scattered mostly in the forward direction. With the forward scattering assumption, Kirchoff's integral can be simplified to yield the complex amplitude at a distance $z$ from the screen, in the following form (Yeh and Liu, 1982)

$$u(\boldsymbol{\rho}, z, t) = \frac{ik}{2\pi z} \int\int e^{-i[\phi(\boldsymbol{\rho}', t) + k|\boldsymbol{\rho} - \boldsymbol{\rho}'|^2/2z]}\, d\boldsymbol{\rho}' \,. \tag{2.16}$$

For weak scintillations, it is useful to write the complex amplitude as follows

$$u(\mathbf{r}, t) = \exp[\chi(\mathbf{r}, t) - iS(\mathbf{r}, t)] \,, \tag{2.17}$$

where $S(\mathbf{r}, t)$ is the phase variation of the wave and $\chi(\mathbf{r}, t)$ is its log-amplitude. For weak scintillations, $\chi \ll 1$, so that changes in amplitude are proportional to changes in $\chi$. In a stochastic description of ionospheric scintillations, one basic assumption is that the phase perturbation $\phi(\boldsymbol{\rho}, t)$ has a Gaussian distribution with zero mean. Then using the expressions for $\chi(\mathbf{r}, t)$ and $S(\mathbf{r}, t)$ based on (2.16), the space-time correlation functions for $\chi$ and $S$ are derived in terms of the power spectrum $S_{\Delta N}(\mathbf{k}, t)$ [ $= \Phi_{\Delta N}(\mathbf{k})\, \Psi(\mathbf{k}, t)$] of the density fluctuations, when the scintillations are weak, i.e., $\langle \phi^2 \rangle \ll 1$. For the case of 'frozen' irregularities, expressions for the spatial correlation functions and the approximations made in deriving them, are described in the review paper by Yeh and Liu (1982). These expressions are given in terms of $\Phi_{\Delta N}(\mathbf{k})$. The temporal correlation functions of $\chi$ and $S$ for a signal received by a single receiver, viz., $B_\chi(0, t)$ and $B_S(0, t)$, are defined in a manner similar to (2.4). These functions involve the time-dependent power spectrum $S_{\Delta N}(\mathbf{k}, t)$. From (2.12), $\Psi(\mathbf{k}, t)$ has the following form for 'frozen' irregularities

$$\Psi(\mathbf{k}, t) = e^{-i\mathbf{k} \cdot \mathbf{V}_0 t} \,. \tag{2.18}$$

The frequency power spectra of $\chi$ and $S$ obtained from temporal variations of the signal transmitted by a geostationary satellite and recorded at a single station are, therefore, given by

$$\Phi_\chi(\Omega) = \frac{2\pi r_e^2 \lambda^2 L}{|V_0|} \int_{-\infty}^{\infty} \Phi_{\Delta N}\left(\frac{-\Omega}{V_0}, k_y, 0\right) \sin^2 \frac{\left(\frac{\Omega^2}{V_0^2} + k_y^2\right) z_R}{2k}\, dk_y \,, \tag{2.19}$$

$$\Phi_S(\Omega) = \frac{2\pi r_e^2 \lambda^2 L}{|V_0|} \int_{-\infty}^{\infty} \Phi_{\Delta N}\left(\frac{-\Omega}{V_0}, k_y, 0\right) \cos^2 \frac{\left(\frac{\Omega^2}{V_0^2} + k_y^2\right) z_R}{2k} \, dk_y , \tag{2.20}$$

in the case of weak scintillations due to 'frozen' irregularities which are convecting with a uniform velocity $\mathbf{V}_0$ in the $x$-direction. For a signal transmitted from an orbiting satellite, which moves at a much greater speed than the irregularity drift, similar expressions are applicable where $V_0$ is now the speed at which spatial variations in the irregularities are scanned by the signal.

For 'non-frozen' irregularities, a general form for the function $\Psi(\mathbf{k}, t)$ suggested by Shkarofsky (1968) is the following

$$\Psi(\mathbf{k}, t) = e^{-i\mathbf{k} \cdot \mathbf{V}_0 t - k^2 \Delta^2/2} , \tag{2.21}$$

where $\Delta$ is the time-dependent r.m.s. displacement of an irregularity in time $t$ due to some decay mechanism. Two special forms of $\Delta$, which may be pertinent in the study of ionospheric scintillations, arise from the decay of irregularities due to fluctuations in their drift velocity and diffusion, respectively. For decay caused by fluctuations in the irregularity drift velocity, it is possible to use a 'locally frozen' field condition when the velocity of individual irregularities changes over a time scale which is long compared with $L_0/V_0$, where $L_0$ is the outer scale associated with the irregularities and $V_0$ is their average drift speed. Further, it is assumed that the velocity fluctuations have a normal distribution with a standard deviation $\sigma_V$ for each velocity component. In this situation, $\Psi(\mathbf{k}, t)$ has been determined to be (Tatarskii, 1971)

$$\Psi(\mathbf{k}, t) = e^{-i\mathbf{k} \cdot \mathbf{V}_0 t - k^2 \sigma_V^2 t^2/2} . \tag{2.22}$$

The process of diffusion also leads to temporal variation of the r.m.s. electric density fluctuation and in this case, $\Delta$ is given by $\Delta = [2D\,|t|]^{1/2}$, where $D$ is the diffusion coefficient (Shkarofsky, 1968). In either case, the space-time correlation function $B_\chi(\boldsymbol{\rho}, t)$, for weak scintillation, is obtained from the phase screen theory (Wernik *et al.*, 1983) as

$$B_\chi(\boldsymbol{\rho}, t) = 2\pi r_e^2 \lambda^2 L \int_{-\infty}^{\infty}\int \Phi_{\Delta N}(\mathbf{k}_\perp, 0) \sin^2\left(\frac{k_\perp^2 z}{2k}\right) \cos[\mathbf{k}_\perp \cdot (\boldsymbol{\rho} - \mathbf{V}_0 t)] \times$$

$$\times e^{-ik_\perp^2 \Delta^2/2} \, d\mathbf{k}_\perp . \tag{2.23}$$

This form of $B_\chi(\boldsymbol{\rho}, t)$ is useful in the analysis of spaced receiver measurements of scintillations.

The $S_4$ index, which is the square root of the normalized variance of intensity, is frequently used as a quantitative measure of the strength of amplitude scintillations on a particular signal. For weak scintillations, it has been shown to have a linear depend-

ence on the r.m.s. density fluctuations in the ionosphere. Rino (1979) has derived a closed form expression for the $S_4$-index when a plane wave is obliquely incident on a phase screen with generally anisotropic irregularities, described by a power-law type of spectrum

$$S_4^2 = r_e^2 \lambda^2 (L \sec\theta) C_S Z^{\nu - 1/2} \left( \frac{\Gamma((2.5 - \nu)/2)}{2\sqrt{\pi}\,\Gamma((\nu + 0.5)/2)\,(\nu - 0.5)} \right] g\,, \qquad (2.24)$$

where $g$ is a combined geometry and propagation factor, $\theta$ is the zenith angle of the signal path, $\nu$ is the power-law index such that $\Phi_{\Delta N}(q) \propto q^{-(2\nu+1)}$ for all wave numbers much larger than cut off wave number, $q_0$, which corresponds to the outer scale of the irregularities. The parameter $Z = \lambda z_R \sec\theta/4\pi$, and $C_S$ represents the strength of turbulence

$$C_S = 8\pi^{3/2} \langle (\Delta N)^2 \rangle\, q_0^{2\nu-2} \Gamma(\nu + \tfrac{1}{2})/\Gamma(\nu - 1)\,. \qquad (2.25)$$

Within the phase screen approximation, (2.24) describes the dependence of weak amplitude scintillations on the spectral index $\nu$ and geometrical facors. It also demonstrates the signal frequency ($f$) dependence of the $S_4$ index.

$$S_4 \propto f^{-(2\nu+3)/4}\,. \qquad (2.26)$$

## 2.3. Rytov solution for weak scintillations

The phase screen approximation does not take into account the effects of propagation of the wave inside the irregularity layer. As the wave propagates through an irregularity slab of finite thickness, amplitude variations build up due to diffraction effects even as the phase varies continuously. Under the forward scattering assumption invoked earlier in the phase screen approach, at any point inside the irregularity layer extending from $z = 0$ to $z = L$, the complex amplitude $u$ of a plane wave, propagating in the $z$-direction, satisfies the following parabolic equation

$$-2ik \frac{\partial u}{\partial z} + \nabla_\perp^2 u = -k^2 \varepsilon_1(\mathbf{r}, t) u\,, \quad 0 < z < L\,, \qquad (2.27)$$

where $\nabla_\perp^2$ is the transverse Laplacian, and $\varepsilon_1(\mathbf{r}, t)$ is the fluctuating part of the dielectric permittivity normalized by the average dielectric permittivity. Once the wave emerges from the irregularity layer, $u$ satisfies the equation

$$-2ik \frac{\partial u}{\partial z} + \nabla_\perp^2 u = 0\,, \quad z > L\,. \qquad (2.28)$$

The time-scale $\tau_c$ for temporal variations of the irregularities is such that the wave frequency $f \gg 1/\tau_c$, and also the time taken by the wave to traverse through the irregularity layer is negligible compared to $\tau_c$. Therefore, no time derivatives appear in (2.27) and (2.28) and $t$ basically plays the role of a parameter which is introduced

through the dependence of $\varepsilon_1$ on time. For solving (2.27) the 'initial' condition at $z = 0$ is given by $u = 1$ for an incident wave of unit amplitude. In order to obtain the solution of (2.28) at $z = z_R$, where the receiver is located, the 'initial' condition is provided by the solution of (2.27) at $z = L$. Once again, $u$ is expressed in terms of $\chi$ and $S$ as in (2.17), and the so-called Rytov solutions for them are obtained in terms of the relevant Green's functions, under the assumption of weak scintillations such that the Born approximation is applicable. Detailed expressions have been given by Yeh and Liu (1982). Frequency power spectra of $\chi$ and $S$ derived from scintillation data of a single station are now given by expressions similar to those in (2.19) and (2.20) in all respects except the Fresnel filter functions $\sin^2[(\Omega^2/V_0^2 + k_y^2)z_R/2k]$ and $\cos^2[(\Omega^2/V_0^2 + k_y^2)z_R/2k]$ which are replaced by

$$\frac{1}{2}\left\{1 \mp \frac{2k}{q^2L}\sin\left(\frac{q^2L}{2k}\right)\cos\left[\frac{q^2}{k}\left(z_R - \frac{L}{2}\right)\right]\right\}, \tag{2.29}$$

where

$$q^2 = \Omega^2/V_0^2 + k_y^2 .$$

In the limit $L \to 0$, (2.29) yields the phase screen Fresnel filter functions as expected. In (2.29), for a given signal wave number, the oscillatory nature of the filter function, which expresses itself in terms of the so-called Fresnel oscillations, is increasingly suppressed for any value of $q$, as the thickness $L$ of the irregularity layer increases (Yeh and Liu, 1982). In the derivation of (2.29), it has been assumed that the background electron density is uniform throughout the irregularity layer, which may not hold generally for the ionosphere.

In a more realistic situation, the background plasma density varies with height in the region of the irregularities with an associated scale height $H$. Adopting an exponential variation of the background density, Liu and Yeh (1977) demonstrated that when the irregularities are confined to a small height interval, variation of the background density does not affect the power spectra. With increasing layer thickness, the background density variation starts playing a greater role. When $H$ is larger than $L$, the Fresnel oscillations are smoothed out, but if $H$ itself is sufficiently small, the power spectra display Fresnel oscillations just as in the case of a thin irregularity layer.

Another important feature of the power spectra of $\chi$ and $S$ is that for a power-law irregularity spectrum of the form $\Phi_{\Delta N}(\mathbf{k}) \propto k^{-p}$, at high frequencies ($\Omega \gg \Omega_F = 2\pi V_0/(2\lambda z_R)^{1/2}$) both $\Phi_\chi(\Omega)$ and $\Phi_S(\Omega)$ show a $\Omega^{-1-p}$ asymptotic power-law dependence. On the other hand, for frequencies much smaller than the Fresnel frequency $\Omega_F$, $\Phi_S(\Omega)$ still exhibits a $\Omega^{1-p}$ behavior, but $\Phi_\chi(\Omega)$ tends to become independent of $\Omega$. A simplified picture of the diffraction process involved (Briggs, 1975) leads to the conclusion that for a power-law irregularity spectrum, irregularities of scale size $d_F \approx (2\lambda z_R)^{1/2}$, which is the dimension of the first Fresnel zone, have the maximum contribution to amplitude scintillations. Thus the width of the transverse spatial correlation function of weak amplitude scintillations is essentially determined by $d_F$.

## 2.4. Multiple scattering regime

The discussion of scintillation theory has so far been restricted to weak scintillations. Expressions obtained under the phase screen approximation are expected to be valid as long as the r.m.s. phase fluctuation, $\langle \phi^2 \rangle^{1/2}$, imposed by the irregularity layer is much less than a radian. The range of validity of the Rytov solution, which is essentially a single scatter solution, extends beyond the 'shallow screen' approximation given by $\langle \phi^2 \rangle \ll 1$ (Keller, 1969). With increasing value of the r.m.s. density fluctuation in the ionosphere, inhomogeneities in the ionospheric refractive index become large enough to cause multiple scattering of the incident wave. This introduces significant changes in statistical characteristics of the scattered wave field, which are determined by moments of the complex amplitude of the wave field. For a complete statistical description of a wave field after propagation through a random medium, it is necessary to calculate all the moments of the wave field.

With (2.27) as a starting point, a complete set of equations satisfied by the moments of the complex amplitude $u$, for different transverse coordinates and different wave numbers, was derived by Lee (1974) under the combined forward scattering and Markov approximations mentioned earlier. From the point of view of scintillation experiments, moments which are of interest are the mutual coherence function (MCF) defined by

$$\Gamma_2 = \langle u(z, \boldsymbol{\rho}, t) u^*(z, \boldsymbol{\rho}', t') \rangle \tag{2.30}$$

and the fourth moment $\Gamma_4$ defined by

$$\Gamma_4 = \langle u(z, \boldsymbol{\rho}_1, t_1) u^*(z, \boldsymbol{\rho}_1', t_1) u(z, \boldsymbol{\rho}_2, t_2) u^*(z, \boldsymbol{\rho}_2', t_2) \rangle \, . \tag{2.31}$$

The wave number dependence of $u$ has been suppressed in the above expressions, since $\Gamma_2$ and $\Gamma_4$ are defined for a single wave frequency.

From the equations satisfied by a general moment of the wave field (Lee, 1974), it is seen that $\Gamma_2$ must satisfy the equation

$$\frac{\partial \Gamma_2}{\partial z} = \frac{-i}{2k} (\nabla_\perp^2 - \nabla_\perp'^2) \Gamma_2 - \frac{4\pi^2 r_e^2}{k^2} [A_{\Delta N}(0, 0) - A_{\Delta N}(\boldsymbol{\rho} - \boldsymbol{\rho}', t - t')] \Gamma_2 \, , \tag{2.32}$$

where $A_{\Delta N}(\boldsymbol{\rho}, t)$ is defined by (2.6). On making the following coordinate transformation in (2.32)

$$\boldsymbol{\xi} = \boldsymbol{\rho} - \boldsymbol{\rho}' \, , \qquad \mathbf{x} = (\boldsymbol{\rho} + \boldsymbol{\rho}')/2 \tag{2.33}$$

and using the fact that $\Gamma_2$ must be independent of $\mathbf{x}$ for a uniform plane wave incident on a homogeneous random medium, (2.32) reduces to

$$\frac{\partial \Gamma_2}{\partial z} = -r_e^2 \lambda^2 [A_{\Delta N}(0, 0) - A_{\Delta N}(\boldsymbol{\xi}, \tau)] \Gamma_2 \, , \quad 0 \le z \le L \tag{2.34}$$

and

$$\frac{\partial \Gamma_2}{\partial z} = 0 \, , \quad z > L \, , \tag{2.35}$$

where $\tau = t - t'$. Equations (2.34) and (2.35) admit the following solution at $z = z_R (> L)$, where the receiver is located.

$$\Gamma_2(z_R, \xi, \tau)) = I_0 \exp\{ - r_e^2 \lambda^2 L [A_{\Delta N}(0, 0) - A_{\Delta N}(\xi, \tau)]\} . \tag{2.36}$$

Here $I_0$ is the intensity of the incident wave. The fact that the MCF is described by a simple analytical expression irrespective of the scintillation strength, makes it a useful statistical parameter to study.

The fourth moment $\Gamma_4$ does not admit such a simple solution. However, it is extremely important as far as scintillation experiments are concerned because the $S_4$-index, as well as the space-time correlation function for intensity scintillations, can be computed from the solution for $\Gamma_4$. For an incident plane wave, the equation satisfied by $\Gamma_4$, when $\boldsymbol{\rho}_1 + \boldsymbol{\rho}_2 - \boldsymbol{\rho}_1' - \boldsymbol{\rho}_2' = 0$, is of the form (Yeh and Liu, 1982)

$$\frac{\partial \Gamma_4}{\partial z} = \frac{-i}{k} \nabla_{\xi_1} \cdot \nabla_{\xi_2} \Gamma_4 - \frac{1}{2L} F(\xi_1, \xi_2, t) \Gamma_4 , \tag{2.37}$$

where

$$\begin{aligned} \xi_1 &= \tfrac{1}{2}(\boldsymbol{\rho}_1 - \boldsymbol{\rho}_2 + \boldsymbol{\rho}_1' - \boldsymbol{\rho}_2') , \\ \xi_2 &= \tfrac{1}{2}(\boldsymbol{\rho}_1 - \boldsymbol{\rho}_2 - \boldsymbol{\rho}_1' + \boldsymbol{\rho}_2') , \\ t &= t_1 - t_2 \end{aligned} \tag{2.38}$$

and

$$\begin{aligned} F(\xi_1, \xi_2, t) = 2 r_e^2 \lambda^2 L \{ & 2A_{\Delta N}(0, 0) - 2A_{\Delta N}(\xi_2, 0) - 2A_{\Delta N}(\xi_1, t) + \\ & + A_{\Delta N}(\xi_1 + \xi_2, t) + A_{\Delta N}(\xi_1 - \xi_2, t)] . \end{aligned} \tag{2.39}$$

Just as in the case of $\Gamma_2$, Equation (2.37) for $\Gamma_4$ has been obtained from the original fourth moment equation by means of a change of variables from $\boldsymbol{\rho}_1$, $\boldsymbol{\rho}_2$, $\boldsymbol{\rho}_1'$, $\boldsymbol{\rho}_2'$ to $\xi_1$, $\xi_2$, $\boldsymbol{\rho}$, and $\mathbf{R}$ where $\boldsymbol{\rho}$ and $\mathbf{R}$ are given by

$$\boldsymbol{\rho} = \boldsymbol{\rho}_1 + \boldsymbol{\rho}_2 - \boldsymbol{\rho}_1' - \boldsymbol{\rho}_2' , \qquad \mathbf{R} = (\boldsymbol{\rho}_1 + \boldsymbol{\rho}_2 + \boldsymbol{\rho}_1' + \boldsymbol{\rho}_2')/4$$

and by recognizing that for a homogeneous random field there can be no dependence on $\mathbf{R}$. There is no loss of generality in setting $\boldsymbol{\rho} = 0$ in the derivation of (2.37), and this is the case which is relevant to the calculation of the space-time correlation function for intensity scintillations, where it is required that $\boldsymbol{\rho}_1 = \boldsymbol{\rho}_1'$ and $\boldsymbol{\rho}_2 = \boldsymbol{\rho}_2'$. Thus it is necessary to simply compute $\Gamma_4(z_R, \xi_1, \xi_2, t)$ for $\xi_1 = \boldsymbol{\rho}_1 - \boldsymbol{\rho}_2$ and $\xi_2 = 0$. The $S_4$-index is further obtained from a special case of this when both $\xi_1$ and $t$ are also set equal to zero. For a plane wave of intensity $I_0$ incident normally on an irregularity slab, the $S_4$-index is related to $\Gamma_4$ through

$$S_4^2 = \Gamma_4(z_R, 0, 0, 0)/I_0 - 1 . \tag{2.40}$$

The normalized space-time correlation function for intensity, of the radio wave received

at $z = z_R$, is given by

$$C_I(\xi, t) = [\Gamma_4(z_R, \xi, 0, t) - 1]/S_4^2 . \tag{2.41}$$

Although (2.37) is not amenable to analytic solution in general, it becomes tractable under the phase screen approximation. In this approach, it is necessary only to solve the equation satisfied by $\Gamma_4$ in the region beyond the irregularity layer

$$\frac{\partial \Gamma_4}{\partial z} = \frac{-i}{k} \nabla_{\xi_1} \cdot \nabla_{\xi_2} \Gamma_4 , \quad z > L , \tag{2.42}$$

with $\Gamma_4(L, \xi_1, \xi_2, t)$ as an initial condition. At the bottom of the irregularity slab ($z = L$), $\Gamma_4$ is computed from (2.15) under the assumption that $\phi(\rho, t)$ has a Gaussian distribution with zero mean. In this manner, an analytic expression has been derived for the spatial power spectrum of intensity fluctuations on the ground due to irregularities which do not vary with time (Shishov, 1974; Rumsey, 1975; Uscinski and Macaskill, 1983). This formulation has been used to model strong ionospheric scintillations produced by a power-law phase screen (Rino, 1979). Asymptotic expressions for $S_4$ and the intensity power spectrum have been derived for large values of $z_R$ and the r.m.s. density fluctuation level, for different values of the power spectral index (Fante, 1976). For a power-law irregularity spectrum of the form

$$\Phi_{\Delta N}(\mathbf{k}) = C_N^2 k^{-p} \tag{2.43}$$

the $S_4$-index is a function of $\zeta = z_R/L_T$ alone where

$$L_T = [8\pi^2(2\pi)^{-p/2} r_e^2 C_N^2 \lambda^{(1+p/2)}]^{(-2/p)} \tag{2.44}$$

represents the dependence on the strength of the irregularities, as measured by $C_N$; the signal wavelength $\lambda$, and the power spectral index $p$. For $p \geq 4$, $S_4$ can exceed unity for certain intermediate values of $\zeta$ beyond which $S_4$ approaches unity with further increase in $\zeta$. This type of behavior has been described as 'focusing' (Gochelashivily and Shishov, 1971) due to refractive scattering (Booker and Majidi Ahi, 1981).

Similar results have also been obtained from numerical solutions of the fourth moment equation (Liu *et al.*, 1974). In these calculations, $\Gamma_4(L, \xi_1, \xi_2, t)$ is obtained numerically by integrating (2.37) through the irregularity slab. In order to simplify the computation, $\rho_1$, $\rho_2$, $\rho_3$, and $\rho_4$ are assumed to lie in a straight line, say along the $x$-axis, in the $z$ = constant plane, so that the vectors $\xi_1$, $\xi_2$ can be replaced by scalars $\xi_1$ and $\xi_2$. Initial condition for the solution of (2.37) is $\Gamma_4(0, \xi_1, \xi_2, t) = 1$. The $S_4$-index and the spatial correlation function for intensity scintillations produced by irregularities which do not vary with time, have been obtained by using a backward difference method to solve (2.37) for a given set of parameters (Liu *et al.*, 1974). As the wave begins to undergo multiple scattering, decorrelation takes place so that the width of the intensity correlation function is no longer determined by the Fresnel filteration process (Yeh *et al.*, 1975). Another effect of multiple scattering is seen in the signal frequency dependence of $S_4$, which now deviates from the weak scintillation result (2.26). For ease of com-

parison with experimental results, the variation of $S_4$ with signal frequency $f$ is assumed to be of the form $S_4 \propto f^{-n}$, where the frequency exponent $n$ has been obtained by computing $S_4$ for different signal frequencies. In agreement with the theory, as the scintillations become stronger the dependence of $S_4$ on $f$ is found to be increasingly weaker as $S_4$ increases (Bhattacharyya *et al.*, 1990). By numerically solving (2.37), Booker *et al.* (1985) have shown that for the computation of the $S_4$-index and the spatial correlation function of intensity, the phase screen approach provides a very good approximation to an extended irregular medium, provided the equivalent screen has the same type of fluctuation spectrum and is centrally located.

For 'non-frozen' irregularities, space-time correlation function of intensity scintillations caused by them has also been obtained by solving (2.37) through a split-step algorithm where the irregularity slab is replaced by a series of phase screens interspersed with diffraction layers (Bhattacharyya and Yeh, 1988). In this manner it is possible to relate the space-time characteristics derived from spaced receiver scintillation measurements, with features associated with random spatial as well as temporal variations of irregularities. For temporal evolution of the irregularities due to decay caused by fluctuations in their convection velocity, an irregularity power spectrum of the form $\Phi_{\Delta N}(\mathbf{k})\psi(\mathbf{k}, t)$ was used with $\psi(\mathbf{k}, t)$ given by (2.22) (Shkarofsky, 1968). The irregularities were considered to be two-dimensional with no variation in the $y$-direction. Then, for spatial separations in the direction of $\mathbf{V}_0$ ($x$-axis), which are much smaller than a characteristic scale length, $l_0$, of the irregularities, and for time separations much smaller than $l_0/\sigma_v$, the intensity space-time correlation function is found to have the form (Franke, 1987; Bhattacharyya *et al.*, 1989)

$$C_I(x, t) = f[(x - V_0 t)^2 + V_c^2 t^2] \,. \tag{2.45}$$

The characteristic velocity $V_c$ is identical to $\sigma_v$ for weak scintillations. As the mean-square phase fluctuation $\langle \phi^2 \rangle$ caused by the irregularity slab increases, there is some deviation of $V_c/\sigma_v$ from unity for intermediate values of $\langle \phi^2 \rangle$. In the region of saturated fluctuations, $V_c/\sigma_v$ asymptotically approaches unity once again as shown in Figure 1.

## 3. Scintillation Experiments

### 3.1. Multifrequency observations

Ionospheric irregularities give rise to maximum phase perturbations on the lowest frequency waves traversing through them. Developments in scintillation theory described in the last section demonstrate that it is much more straightforward to derive turbulence parameters from weak scintillation data than from observations of strong scintillations. However, it becomes necessary to understand features of strong scintillations when density fluctuations in the ionosphere become so large that the radio wave monitored in a given experiment undergoes multiple scattering. In this context, simultaneous observations of scintillations on waves of different frequencies assumes a great deal of importance.

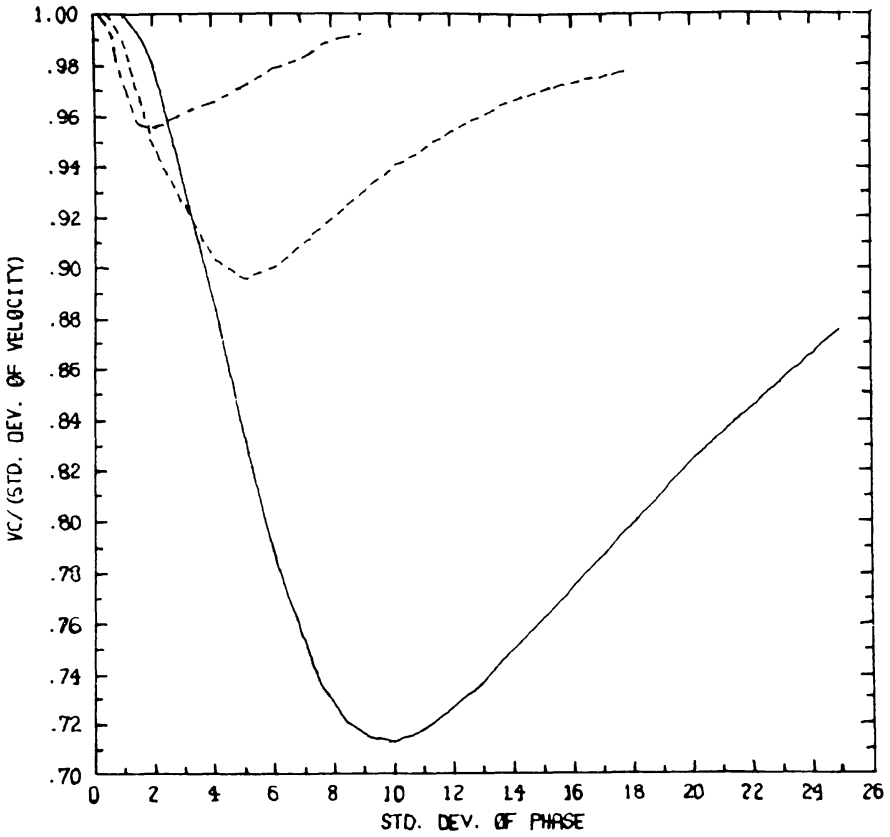


Fig. 1. Dependence of $V_c/\sigma_v$ on the standard deviation $\sigma_\phi$ of phase fluctuations caused by the irregularity slab. Two-dimensional irregularities with a power-law type of spectrum with index $p$ are considered. Solid line represents $p = 4$, short-dashed line represents $p = 3$ and long- and short-dashed line represents $p = 2$ (Bhattacharyya *et al.*, 1989).

There have been a number of such experiments in the past. One of the first such observations was carried out for linearly polarized radio waves of frequencies 40, 140, and 360 MHz transmitted from the ATS-6 satellite (Davies *et al.*, 1975). There were two phases of the ATS-6 experiment. In the first phase, this geostationary satellite was parked at 94° W, and amplitude scintillations on the three frequencies were recorded at Boulder (40.13° N, 105.24° W) (Umeki *et al.*, 1977a, b) and at the dip equatorial station Huancayo (11.96° S, 75.34° W, dip latitude 0.6° N) (Basu *et al.*, 1977). In addition to the amplitudes, phase quadrature components of 40- and 140-MHz signals were also recorded at Boulder using the 360-MHz signal as reference (Myers *et al.*, 1979). In the second phase of the experiment, ATS-6 was positioned at 35° E during the period from August 1975 to July 1976, when measurements were made of the amplitudes of 40-, 140-, and 360-MHz signals and the phase-quadrature components of 40- and 140-MHz signals at the dip-equatorial station Ootacamund (11.4° N, 76.7° E, sub-ionospheric dip 4.4° N). Some of the results obtained from the ATS-6 experiment are described in the next section.

In 1976, the satellite P76-5 was launched into a near-polar orbit at a height of 100 km, to study ionospheric scintillations using a coherent radio beacon (DNA-002), that transmitted circularly polarized signals at ten frequencies which were harmonics of

11.4729 MHz. The available frequencies, viz., one VHF, seven UHF, one *L* band and one *S* band, ranged from 137.6748 to 2891.171 MHz. The signals were received at two low-latitude stations: Ancon (dip 0.4° N) and Kwajalein (dip 4.4° N); one mid-latitude station Stanford (dip 42.8° N); and at Poker Flat (dip 65.4° N) in the auroral region. The high stability of the Sun-synchronous orbit of the satellite allowed repeated pre-midnight observations at low latitudes and near-midnight observations at auroral latitudes.

The geostationary communications satellite, MARISAT located at 15° W, transmitted signals at 254 MHz, 1541.5 MHz (*L* band) and 3945.5 MHz (*C* band). Using these transmissions, simultaneous scintillation measurements at VHF and GHz were made at Huancayo (dip 0.6° N) (Mullen *et al.*, 1977). In early 1981, amplitude scintillations on the MARISAT signals were recorded at Ascension Island (7.95° S, 14.42° W, 30° S dip) which is situated near the southern crest of the Appleton anomaly in *F*-region ionization (Franke *et al.*, 1982, 1984). Mid-latitude ionospheric scintillations, occurring under different geophysical conditions, have been studied extensively using 136 MHz, 1.7 GHz, and 11.5 GHz transmissions from the geostationary satellite ETS-II stationed at 130° E (Ogawa *et al.*, 1980; Fujita *et al.*, 1982). These signals were recorded along with gigahertz signals from two other geostationary satellites, parked at 135° E and 140° E, respectively, at three Earth stations: Kashima (35°57′ N, 140°40′ E), Kokubunji (35°42′ N, 139°29′ E) and Hatoyama (35°58′ N, 139°19′ E). These are some of the multifrequency observations which have been utilized to extract information about ionospheric irregularities in different latitudinal regions.

### 3.2. Spaced-receiver observations

Effects of 'non-frozen' behavior of ionospheric irregularities, such as random temporal fluctuations in their drift velocity, are neglected in the analysis of scintillation data collected at a single receiver. This is acceptable because only the high frequency part of the scintillation spectrum is susceptible to non-frozen flow effects (Wernik *et al.*, 1983), and there is only a minor contribution to the observed scintillations from this part of the spectrum. In order to study the 'non-frozen' aspect of ionospheric irregularities, it is therefore necessary to make spaced-receiver observations of scintillations produced by them. Such measurements have been used for decades to deduce ionospheric drifts. Even assuming that the irregularities are 'frozen', spaced receiver measurements are required to deduce quantitatively, the anisotropy, or the height of the irregularity layer, from scintillation data.

Use of the spaced-receiver analysis technique was demonstrated with scintillation data for a UHF signal, from the Wideband satellite, recorded by a four-receiver system at the high latitude station of Poker Flat (Rino and Livingston, 1982). In this experiment involving transmissions from an orbiting satellite, ionospheric irregularities were assumed to be 'frozen', and instead the complex relationship between apparent drifts and the anisotropy of the diffraction pattern, arising due to the anisotropic nature of the random medium, was explored. A similar study was carried out by Costa *et al.* (1988)

using a 250-MHz transmission from a quasi-geostationary polar beacon, which was recorded by three spaced receivers at Goose Bay (53.3° N, 60.3° W); and using a 413 MHz signal transmitted by the polar-orbiting Hilat satellite, which was recorded by three receivers at Tromsø (69.7° N, 18.9° E).

In the mid-latitudes, three station observations of amplitude scintillations on a 40-MHz transmission from the satellite Explorer 22 were made at London, Ontario (43.0° N, 81.3° W) and at Delaware, Ontario (42.9° N, 81.4° W), as early as 1968 (Moorcroft and Arime, 1972). The ground diffraction patterns were interpreted to give statistical results for certain irregularity features such as height, size, and shape, assuming axially symmetric, field-aligned, 'frozen' irregularities. More recently, the behavior and dynamics of mid-latitude irregularities have been investigated using three closely spaced antennas at Hiraiso (36°22′N, 140°37′ E, dip 26.3° N) to observe scintillations on a 136-MHz signal from the geostationary satellite ETS-II (Kumagai *et al.*, 1982; Kumagai and Ogawa, 1986).

The first attempt to include 'non-frozen' behavior of ionospheric irregularities in modeling spaced-receiver scintillation measurements was made with observations carried out at Ancon (dip 2° N) near the magnetic equator (Wernik *et al.*, 1983). This study utilized data obtained from three receivers which monitored a 249-MHz signal from the near-geostationary satellite LES 9. As part of the Project Condor equatorial spread *F* campaign during 1983, spaced receivers at Ancon recorded amplitude scintillations on a 244-MHz signal transmitted from the geostationary Fleetsatcom satellite. This signal was also monitored at another equatorial station. Huancayo, by a spaced receiver system (Basu *et al.*, 1986). Further studies of random temporal variations in equatorial ionospheric irregularities have been carried out using amplitude scintillation data for a 250-MHz transmission from the geosynchronous Pacific Fleet satellite located at 176.5° E, which was recorded by two spaced receivers at Guam (12.4° N, 147° E, dip 4.8° N) (Vacchione *et al.*, 1987; Spatz *et al.*, 1988; Bhattacharyya *et al.*, 1989).

### 3.3. Multi-technique observations

The inadequacy of scintillation data to resolve various parameters of the ionospheric irregularities that cause the scintillations has, sometimes, been overcome by supplementing scintillation measurements with coordinated *in situ* and radar observations (Basu *et al.*, 1980). For instance, one-dimensional sampling of the ionospheric density fluctuations by probes on board rockets and satellites, in fact, provided direct evidence for power-law type of irregularity spectra in the equatorial ionosphere, which are widely used in modeling scintillation observations. Spectral characteristics of medium-scale equatorial *F*-region irregularities have been studied by launching a rocket equipped with a four frequency phase-coherent beacon, and *in situ* probes to measure plasma density and electric field, into active equatorial spread *F* (Rino *et al.*, 1981; Livingston *et al.*, 1981). A coordinated study of scintillations arising due to bottomside sinusoidal (BSS) irregularities in the equatorial *F*-region, which were identified in data from the Atmosphere Explorer E (AE–E) satellite, allowed an estimation of the apparent transverse drift of the BSS irregularities (Basu *et al.*, 1986).

The operating frequencies of radars are generally so high that the scattered radio waves give direct information pertaining to short wavelength ($\sim$ few meters) density fluctuations only. Such short wavelength irregularities do not contribute to observed ionospheric scintillations on account of the power-law nature of ionospheric irregularity spectrum, and the diffraction process involved in the phenemenon of scintillation. Nevertheless, in the equatorial region, it has been established theoretically that the short wavelength irregularities are generated by plasma instabilities which grow on the density gradients associated with the large-scale irregularities (Haerendel, 1974). Thus, the presence of short scale length density fluctuations in a region of the ionosphere indicates the presence of large scale irregularities. This is the raison d'etre of coordinated radar and scintillation observations. It is, however, possible for long wavelength irregularities which give rise to scintillations to be present even when no radar backscatter is observed, indicating the non-existence of short wavelength irregularities (Basu *et al.*, 1978). One of the most exhaustive multi-technique observations carried out in recent times was the Project Condor equatorial spread-*F* campaign. In this campaign, 50-MHz radar observations were carried out at the Jicamarca Radio Observatory (JRO) together with VHF and UHF scintillation measurements at Ancon. Spaced receiver measurements of VHF scintillations were also made at Ancon, where a 14-MHz radar was operated. Use was also made of data from a digital ionosonde, magnetometer data and ionogram records obtained at Huancayo, and Fabry–Pérot interferometer data recorded at Arequipa, in the equatorial region. Two rocket-borne payloads were launched from the Punta Lobos rocket range during times of active spread F as indicated by radar data (Kelley *et al.*, 1986). Some of the results obtained from these measurements (Basu *et al.*, 1986) are discussed later.

In the equatorial region, simultaneous, large scale, coordinated observations of ionospheric irregularities using different techniques have been undertaken on a number of occasions. However, in the mid-latitude regions, there is a paucity of such measurements. Even in high-latitude regions, there are few such observations. There have been simultaneous measurements of low-energy ($<500$ eV) electron precipitation in the auroral oval from DMSP/F2 satellite and phase and amplitude scintillations on a 244-MHz signal from Fleetsat satellite recorded at Goose Bay (Basu *et al.*, 1983). Also coordinated observations of auroral zone plasma enhancements have been carried out using radio, optical and scintillation measurements on a series of north–south flight legs of AFGL's airborne ionospheric observatory along the magnetic meridian of the Chatanika incoherent scatter radar (65.1° N, 147.5° W). At the same time the radar was used to scan the ionosphere along the north–south magnetic meridian and ionospheric parameters such as electron density, temperature, and ion drift were obtained over a range of altitudes (Weber *et al.*, 1985). A study has also been made of the precise contributions that a satellite-borne irregularity sensor can make towards the proper modeling of scintillation observations. For this purpose, use was made of the Dynamics Exporer 2 (DE 2) satellite data for electron density in the irregularity region over the winter polar cap, collected during sunspot maximum conditions, while polar beacon satellite measurements were made at 250 MHz. At the same time, an all-sky imaging

photometer was deployed at Thule, Greenland, within the polar cap, to monitor the presence of convecting ionization patches (Basu *et al.*, 1988). Such multi-technique observations have played an important role in the utilization of scintillation data for extracting information about ionospheric turbulence.

## 4. Irregularity Parameters from Scintillation Measurements

### 4.1. Power spectral studies

According to the theory of scintillations reviewed in Section 2, basic shape of the power spectra of weak amplitude and phase scintillations is determined directly by the shape of the power spectrum of ionospheric irregularities which give rise to these scintillations. Fresnel diffraction effects are superimposed on this basic shape. As a result of Fresnel filteration, it is expected that the power spectra of weak amplitude scintillations will deviate from that of weak phase scintillations for frequencies less than the Fresnel frequency $\Omega_F$ ($= 2\pi V_0/\sqrt{2\lambda z_R}$) where $V_0$ is the average drift speed of the irregularities transverse to the signal path and $z_R$ is the effective distance along the signal path, of the iregularity layer from a receiver. For an irregularity power spectrum of the power-law form, at frequencies greater than $\Omega_F$, there should be a power-law fall off for both the amplitude and phase power spectra. For strong scintillations, there is no direct relationship between temporal scales associated with scintillations and irregularity scale sizes as in the case of weak scintillations. However, a large volume of scintillation data falls in this category. Numerical simulation has proved to be a useful tool in the extraction of information about ionospheric irregularities from strong scintillation data (Franke and Liu, 1983).

#### 4.1.1. *Amplitude Scintillations*

A power-law behavior for the power spectrum of amplitude scintillations due to ionospheric irregularities was first reported for observations made in a sub-auroral region (Elkins and Papagiannis, 1969). Furthermore, on the basis of theory, it was recognized that from the slope of the high-frequency asymptotes of log-log plots of scintillation power spectra, it is possible to deduce the spectral index $p$ ($= m + 1$) for the three-dimensional irregularity power spectrum of the power-law form. A study of the power spectra of amplitude scintillations recorded at a mid-latitude location, demonstrated that the ionospheric *F*-region irregularities there must have a power-law wave number spectrum (Rufenach, 1972). Since then there have been a large number of power spectral studies of amplitude scintillations monitored in different parts of the globe (Singleton, 1974; Crane, 1976; Umeki *et al.*, 1977; Fremouw *et al.*, 1978; Franke and Liu, 1983; Bhattacharyya and Rastogi, 1985; Basu *et al.*, 1986). In Figure 2, power spectra computed from amplitude scintillation data for 40- and 140-MHz signals recorded at Boulder are compared with theoretical power spectra.

In the power spectrum of weak amplitude scintillations, there is often a broad maximum around the Fresnel frequency, and therefore, only a rough estimate of $\Omega_F$ can

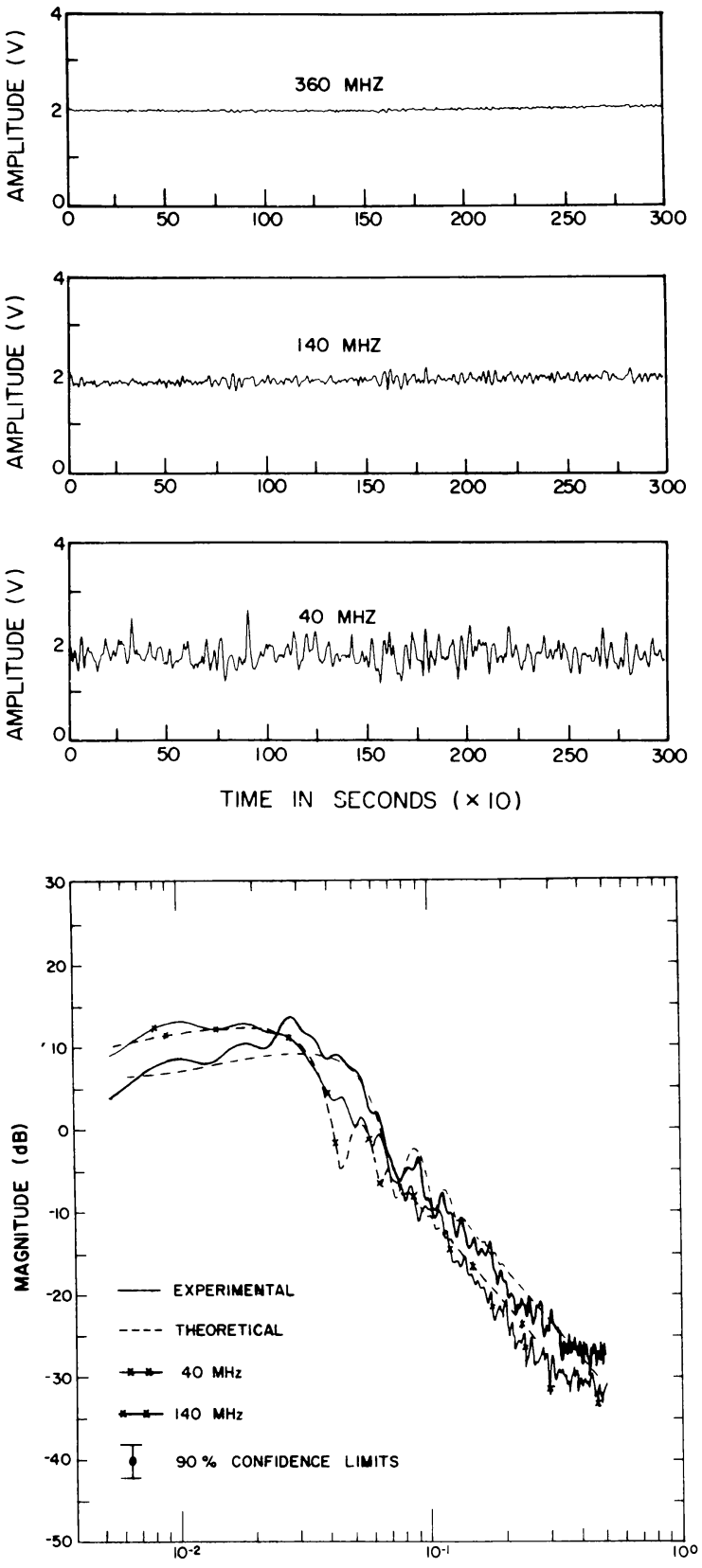


Fig. 2. (a) Amplitude scintillations on 40-, 140-, and 360-MHz signals from the ATS-6 satellite (94° W) recorded at Boulder (40.13° N, 105.24° W).

be obtained from it. It is not possible to determine $V_0$ from scintillation data of a single station, unless a value is assigned to $z_R$. Even if a reasonable value of $z_R$ is used, as is possible for daytime scintillations, the uncertainty in $\Omega_F$ does not allow accurate determination of $V_0$. However, it is necessary to have an idea of $V_0$ in order to convert the frequency scale to a wave number scale for weak scintillations, so that features of the irregularity spectrum can be associated with the appropriate irregularity scale lengths. Then, besides the power spectral index associated with a power-law irregularity spec-

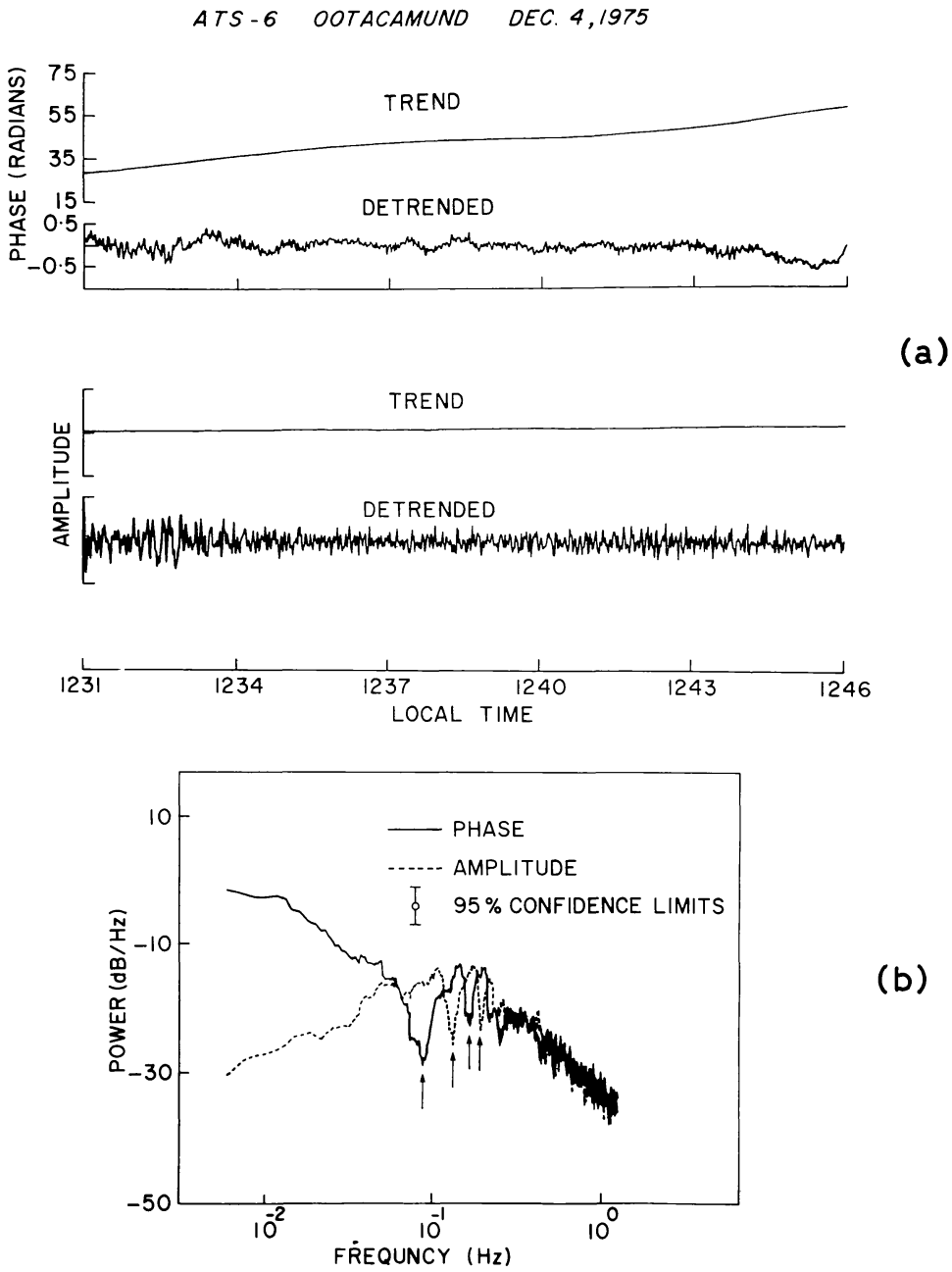


Fig. 3. (a) Detrended phase and amplitude scintillation data recorded at an equatorial station, Ootacamund (subionospheric dip 4.4° N). (b) Smoothed power spectra of the detrended scintillation data. First few Fresnel minima are indicated by arrows (Bhattacharyya, 1991).

trum, the range of irregularity wavelengths for which this power-law form is applicable, can also be determined from amplitude scintillation data.

According to the Rytov solution for weak scintillations, when these are caused by a sufficiently thin layer of irregularities, it should be possible to discern Fresnel oscillations in the power spectra of scintillations. This situation has been found to exist in the dip equatorial region under two different circumstances. The first one is during daytime, when scintillations are caused by irregularities in the electrojet region of the ionosphere. An example of a power spectrum of daytime amplitude scintillations, observed at an equatorial station, which exhibits pronounced Fresnel oscillations is shown in Figure 3

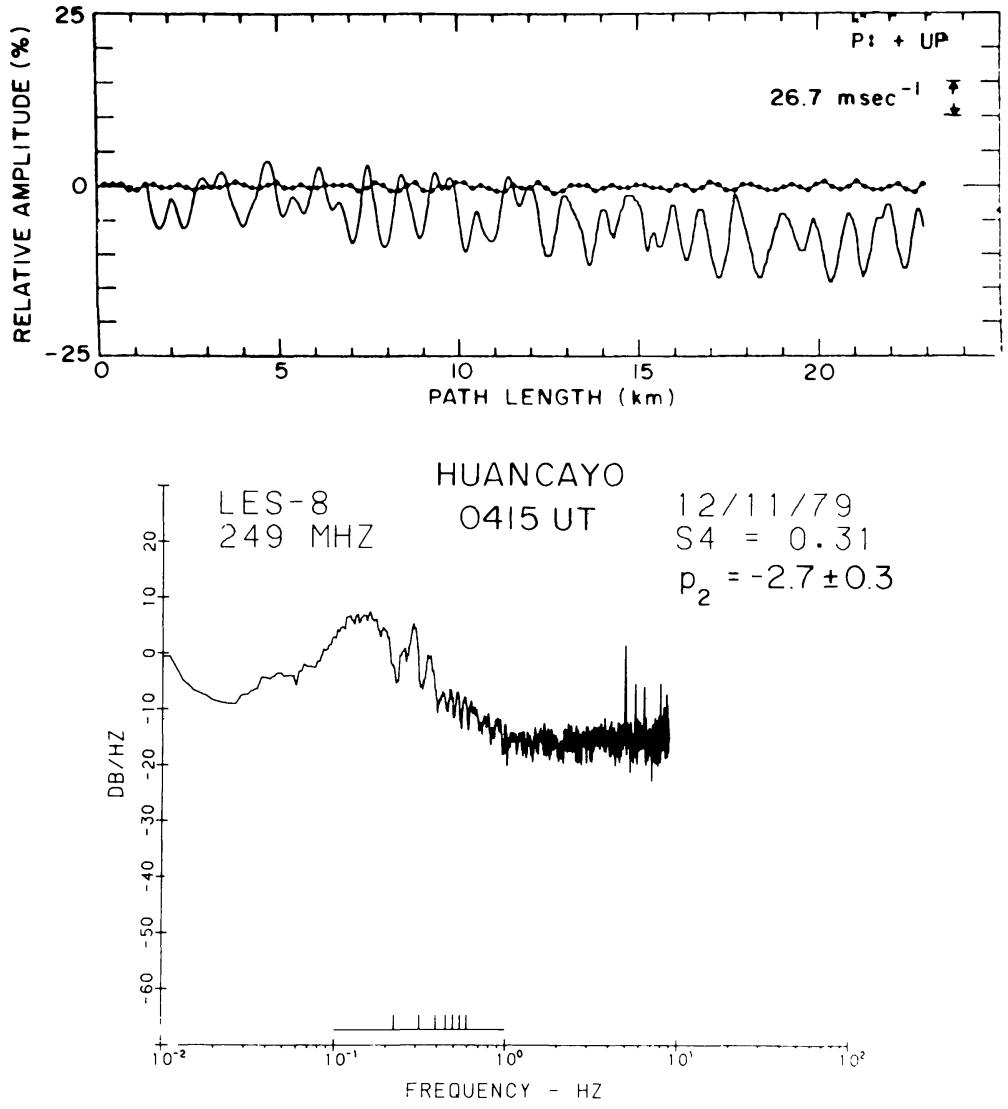


Fig. 4. (a) Fluctuations of ion density (solid curve) recorded by a retarding potential analyzer during a 3-S interval starting at 04:49:30 UT on December 11, 1979, for AE–E orbit 22700 when it passed through BSS irregularities near the Huancayo longitude sector. The curve with solid circles represents the pitch or vertical drift from the ion drift meter. (b) The spectrum of amplitude scintillations on a 249 MHz signal from LES 8 observed at Huancayo in the presence of BSS irregularities of the type shown in (a). Frequencies of the first seven Fresnal minima are indicated by the scale above the frequency axis and $p_2$ is the computed power law index of the roll-off portion of the spectrum (Basu *et al.*, 1986).

(Bhattacharyya and Rastogi, 1986). It is seen that, in addition to the Fresnel maxima, the Fresnel minima are also very well defined and the $n$th minimum occurs at a frequency $\Omega_{an} \propto \sqrt{n}$, as expected from weak scintillation theory. These minima at $\Omega_{an} = V_0(n/\lambda z_R)^{1/2}$, therefore, provide a fairly accurate estimate of $V_0$ if $z_R$ is known to a reasonable degree of accuracy. The other case, depicted in Figure 4, where Fresnel oscillations are clearly evident, is for scintillations associated with bottomside sinusoidal (BSS) irregularities in the equatorial $F$-region (Basu *et al.*, 1986). Here, the presence of Fresnel oscillations indicates that the BSS irregularities are confined to a relatively thin layer.

Weak amplitude scintillations on VHF and higher frequencies can only yield information about irregularities of scale sizes less than 1 km because of Fresnel diffraction. On the other hand, strong scintillations contain information about irregularities with spatial sizes much greater than the Fresnel dimension ($= \sqrt{2\lambda z_R}$) because of refractive scattering. With this in view, Franke and Liu (1983) resorted to numerical simulations to model strong scintillation events. A random one-dimensional phase screen with a prescribed power spectral density function is generated numerically, and the resultant wave field on the ground due to this screen is computed. It is necessary to use an irregularity drift speed to convert spatial fluctuations on the ground to temporal fluctuations. Comparisons of modeling results (Figure 5) with obervations of multifrequency VHF and GHz scintillations in the equatorial region clearly indicated the necessity of describing $F$-region irregularities by a two-component power-law spectrum, with a shallow large-scale regime and a steeper small-scale regime with the break in spectral slope occurring at a scale size of the order of a kilometer. This result was in agreement with those derived from *in situ* measurements of density variations along the vertical and magnetic east–west directions in the equatorial $F$-region (Rino *et al.*, 1981; Kelley *et al.*, 1982; Basu *et al.*, 1983). This two-component nature of the irregularity power spectrum was further corroborated in a later study of the signal frequency dependence of the $S_4$-index (Franke *et al.*, 1984).

At high-latitudes 137-MHz beacon signals from the HILAT satellite have been recorded at the Polish Polar Station at Hornsund, Svalbard (invariant latitude $\Lambda = 73.4N$) since 1984 (Wernik *et al.*, 1990). Amplitude scintillation spectra computed using these data show a pronounced dependence on the geometry of the propagation path with respect to the magnetic field. Wernik *et al.*, showed that anisotropic irregularity spectra with different spectral indices along and across the magnetic field line can explain the observations. Their results indicate that, in order to understand the high-latitude irregularity structure, three-dimensional numerical simulations of the irregularity evolution are needed.

### 4.1.2. *Phase Scintillations*

Global phase scintillation data is meagre in comparison to amplitude scintillation data, because of the complexities involved in the measurement of phase. In the analysis of phase data, it has to be borne in mind that density variations in the ionosphere span a large range of scale sizes extending over 6 to 7 orders of magnitude, and, therefore

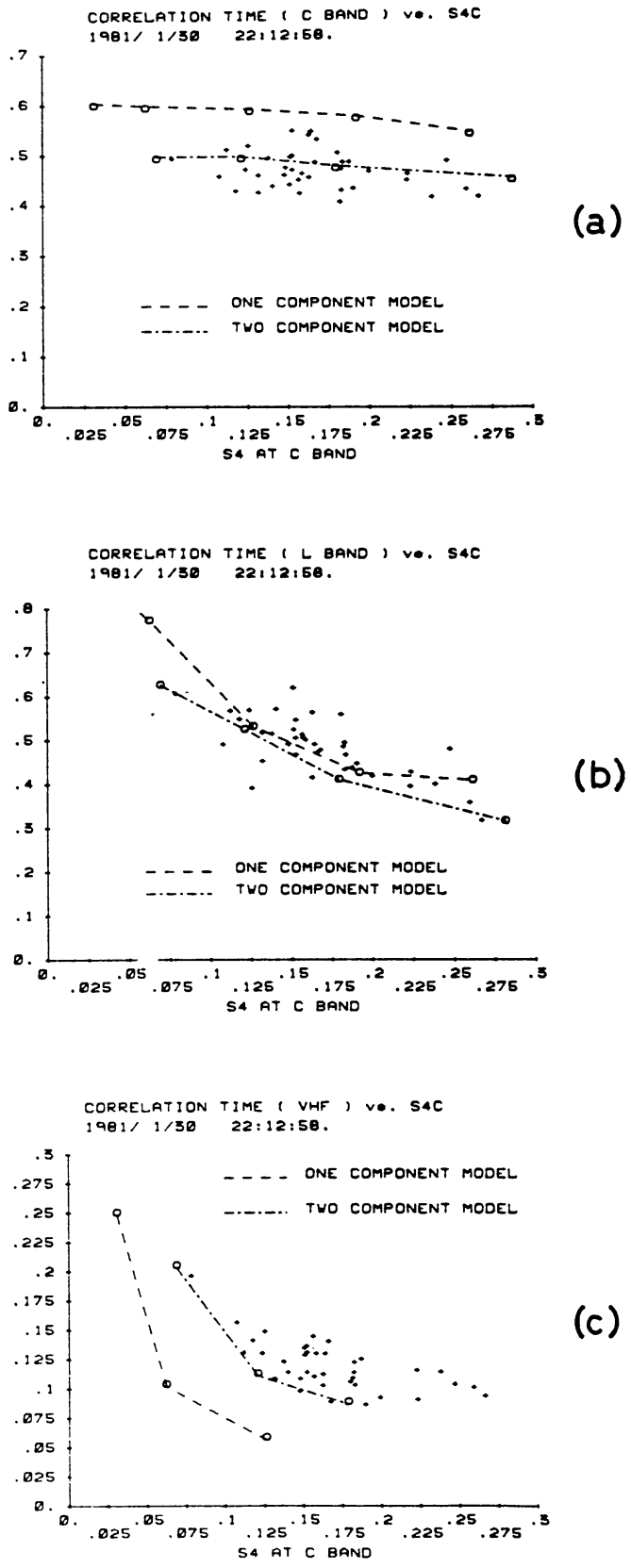


Fig. 5. Correlation time (time to 50% decorrelation) at (a) C band, (b) L band, and (c) VHF versus $S_4$ at C band. The crosses represent the experimental data points – each point was computed from 1 min of data. The dotted lines show the numerical simulation results (Franke and Liu, 1983).

phase perturbations imposed by them on an incident radio wave also have such an extended spatial spectrum. Amplitude scintillations, on the other hand, do not contain low-frequency components because of Fresnel filteration in the case of weak scintillations, and because 'focusing' in the strong scintillation regime causes large-scale irregularities to give rise to small scale variations of amplitude. Computation of statistical parameters from scintillation data calls for stationarity of the data. This requirement necessitates the introduction of a criterion for detrending the phase data where fluctuations in phase, which are as fast or faster than the slowest amplitude variations, are included in phase scintillations and slower variations of phase are considered as trend (Fremouw *et al.*, 1978). Power spectra of phase scintillations have been studied in the high latitude (Fremouw *et al.*, 1978, 1985); mid-latitude (Myers *et al.*, 1979) and in the equatorial region (Bhattacharyya and Rastogi, 1986; Bhattacharyya, 1990).

Power spectra of weak phase scintillations can be used directly to extract information about irregularities of scale sizes larger than the Fresnel dimension, which do not contribute to weak amplitude scintillations. Such a study has brought to light unexpected spectral behavior of phase scintillation in the nighttime auroral region, which could have a possible explanation in terms of size-dependent anisotropy (Fremouw *et al.*, 1985). It has been suggested that such a scale-size dependent anisotropy could be initiated by structured, soft electron precipitation setting up *L*-shell aligned, latitudinally non-uniform structures in the *F*-layer (Muldrew and Vickrey, 1982; Rino and Owen, 1980; Leitinger *et al.*, 1982). Smaller-scale structure would then arise from these large-scale structures through a cascade process involving a convective instability.

For the equatorial *F*-region, power spectra computed from phase scintillations were utilized to determine the long- and short-wavelength spectral indices and the break scale length at which the transition from a shallow to a steep slope occurs. These estimated parameters were introduced in a model calculation of the dependence of the $S_4$-index on signal frequency, using weak scintillation theory. A comparison of the computed signal frequency dependence of the $S_4$-index with that obtained from multi-frequency observations of amplitude scintillations demonstrated the degree of accuracy of the estimated parameters (Bhattacharyya and Rastogi, 1986). Thus, simultaneously recorded amplitude and phase scintillation data could establish unambiguously the two-component nature of the irregularity power spectrum in the intermediate range of wavelengths (100 m to a few km) in the equatorial *F*-region. The origin of the apparent break in the irregularity spectrum is now attributed to the evolution of the generalized Rayleigh–Taylor instability in the equatorial *F*-region into a highly anisotropic state (Zargham and Seyler, 1987). This state is characterized by nearly sinusoidal variations in density along the direction of an effective electric field prevalent in the region, and shock-like structures propagating perpendicular to this direction. Thus a one-dimensional sampling of the density variations as in rocket or satellite observations, or in the scintillation phenomenon, can yield a two-component power-law spectrum for the irregularities depending on the angle between the signal path and the effective electric field (Kelley *et al.*, 1987).

### 4.2. Correlation analysis of spaced-receiver data

Weak scintillations recorded by a single receiver can be directly used to deduce power spectral indices associated with the irregularity spectrum, whereas other irregularity parameters such as the height, degree of anisotropy, etc. can only be obtained indirectly on the basis of a particular model of the irregularities (Umeki *et al.*, 1977). Likewise, numerical simulation studies of strong scintillations (Franke and Liu, 1983, 1985) lead to indirect information about ionospheric turbulence. Spaced receiver scintillation measurements, on the other hand, can provide more information about the irregularities, such as the average drift speed of the irregularities, their anisotropy and their non-frozen behavior caused by velocity fluctuations, diffusion, etc. Some results obtained from the analysis of such data are summarized below, for different latitudinal regions.

#### 4.2.1. *High-latitudes*

Present-day correlation analysis of spaced receiver data has as its precursor the method of similar fades (Mitra, 1949) whereby ionospheric drifts were estimated by measuring the time delay between the arrival of two similar structures at two spaced receivers. The drift component along the axis joining the receivers, derived from the time lag of maximum cross-correlation between signals recorded at the two receivers, does not give the true drift when random temporal changes take place in the diffraction pattern due to 'non-frozen' behavior of the irregularities or when the irregularities are anisotropic (Briggs *et al.*, 1950).

In the nighttime auroral region, spaced-receiver data confirmed the hypothesis that the diffraction pattern, due to ionospheric irregularities in this region is elongated along the geomagnetic east–west direction whenever an enhancement in radio wave scintillations is observed (Rino *et al.*, 1978). Further, the phase fluctuations $\delta\phi(\mathbf{r}, t)$, of a transionospheric signal received on the ground, are related to ionospheric density fluctuations $\Delta N(\mathbf{r}, t)$ through geometrical optics, and the irregularities are considered to be 'frozen' in order to interpret measured variations in anisotropy and diffraction pattern drift (Rino and Livingston, 1982). These results demonstrate the complicated relationship between apparent drifts and the anisotropy of the diffraction pattern due to an anisotropic random medium. This complex dependence of apparent drift on anisotropy has been explored in detail by using different algorithms for the cross-correlation analysis of spaced-receiver data from the high latitude region (Costa *et al.*, 1988).

For a system of $n_r$ receivers on the ground located at $\boldsymbol{\rho}_i = (x_i, y_i)$, $i = 1, 2, \ldots, n_r$, all the auto- and cross-correlation functions $B(\boldsymbol{\rho}_i - \boldsymbol{\rho}_j, \Delta t)$ are computed. These are modeled by a function of $(\boldsymbol{\rho}_i - \boldsymbol{\rho}_j)$ and $\Delta t$ combined into a quadratic form such that surfaces of constant-correlation are concentric ellipsoids. The parameters that characterize the correlation ellipsoids can then be estimated from spaced receiver data by using time delays for intersection of various correlation functions (Briggs, 1968). Geometry of the scintillation problem for irregularities in the high latitude region is sufficiently complex that initroduction of 'non-frozen' behavior of the irregularities would not allow for a simple interpretation of the spaced-receiver observations. Hence the assumption

of 'frozen' irregularities is made. Analysis of data from a quasi-stationary polar beacon has shown the occurrence of large daily variations in the anisotropy of the ground diffraction pattern and in the true drift velocity of ionospheric irregularities (Costa *et al.*, 1988). On the other hand, spaced-receiver records of scintillations on a signal from an orbiting satellite have demonstrated geometrical enhancements in the $S_4$-index, in the r.m.s. phase fluctuation, and in the axial ratio of the ellipse that characterizes the

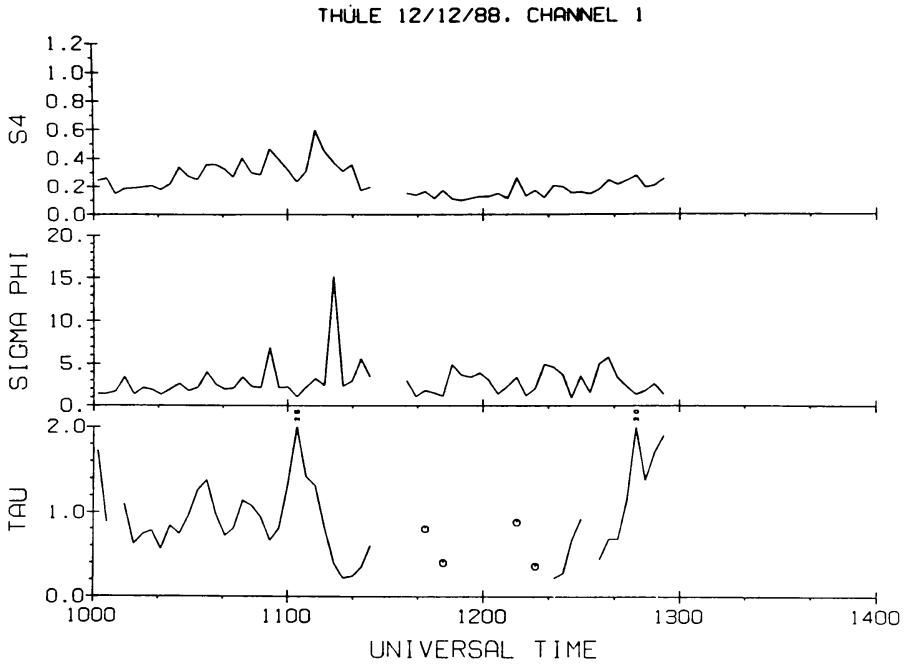


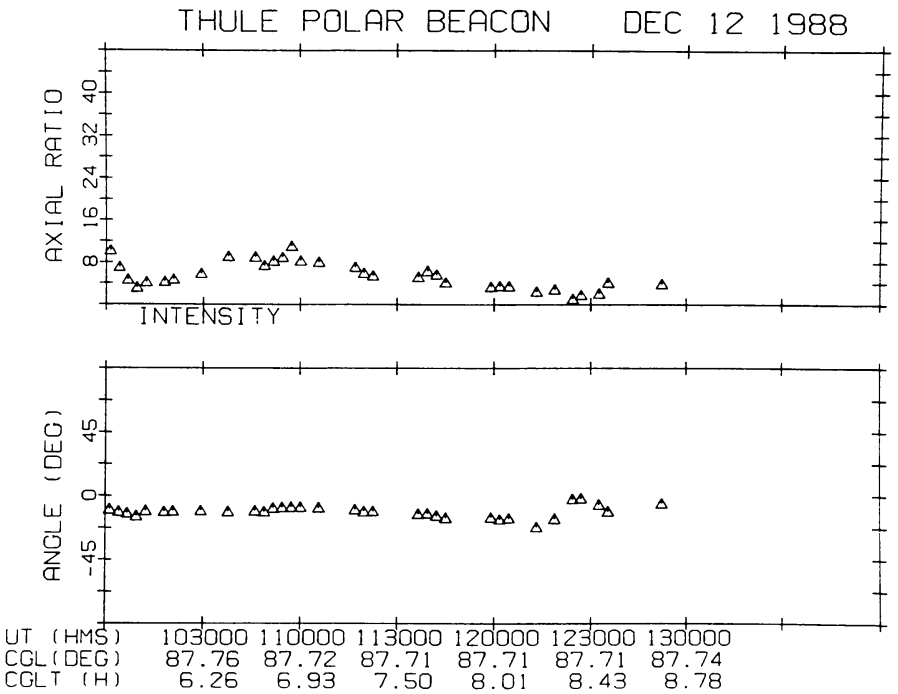

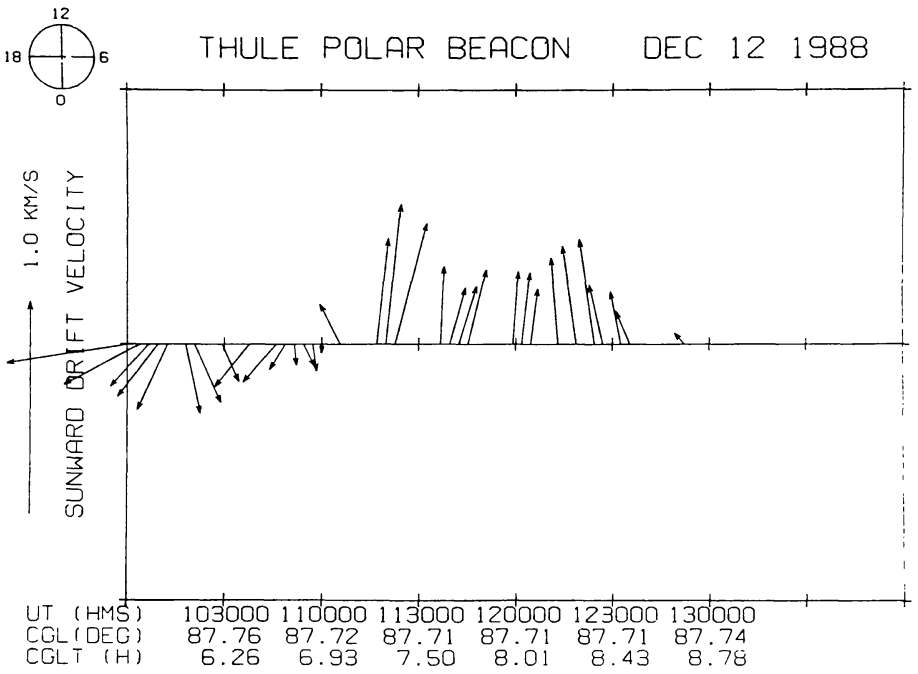


Fig. 6. (a) $S_4$-index; $\sigma_\phi$, the standard deviation of phase scintillations; and decorrelation time for a 250 MHz signal observed at Thule in conjunction with Sun-aligned arcs on December 12, 1988. (b) Axial ratios and orientation angles of the anisotropy ellipses of the diffraction pattern obtained from spaced-receiver intensity data corresponding to the time interval indicated in (a). (c) Magnitudes and directions of the true drift velocity of the diffraction pattern corresponding to the same time interval. The direction towards the Sun at magnetic noon is indicated. Clear reversal of the drift velocity from antisunward to sunward is seen (Basu *et al.*, 1991).

anisotropy of the ground diffraction pattern, in the vicinity of local $L$ shell alignment of the ray paths (Costa *et al.*, 1988). Spaced-receiver scintillation measurements have been carried out at Thule and Sondrestrom, Greenland, for a 250-MHz signal transmitted from a quasi-geostationary polar beacon satellite, to study the control of small-scale irregularities in the polar cap ionosphere by the north–south component of the interplanetary magnetic field (IMF) (Basu *et al.*, 1991). Some results obtained at Thule are shown in Figures 6(a), (b), and (c). The authors found that the strength of $F$-region irregularities, their anisotropy, and drifts within the polar cap are controlled by the orientation of the IMF $B_z$ component.

### 4.2.2. *Mid-latitudes*

Diffraction effects must be taken into account for an accurate description of amplitude and phase fluctuations recorded on the ground, in terms of density variations in the ionosphere. Hence, it is necessary to go beyond geometrical optics for interpreting spaced-receiver scintillation data. As discussed earlier, the space-time correlation function of intensity scintillations can be computed by solving the appropriate fourth moment equation. Mid-latitude nighttime scintillations on a VHF signal recorded by three closely spaced antennas, under geomagnetically quiet conditions, were subjected to correlation analysis (Kumagai and Ogawa, 1986). As in the case of high-latitude

observations, the correlation analysis was based on the assumption that the surfaces of constant correlation were approximately ellipsoidal (Briggs, 1968). Thus, at a particular instant of time, contours of constant correlation on the observation plane at ground level are ellipses. Characteristics of these ellipses, such as the orientation of the major axis, the axial ratio, and the length of the minor axis were derived from three pairs of auto- and cross-correlation functions by using time delays at which correlation functions have the value of 0.5. Kumagai and Ogawa (1986) found that in the pre-midnight hours, the drift was mostly in the southward or south–westward directions, while in the post-midnight hours, the percentage of northward drifts increased. Occasionally, very large northward drifts were observed during the post-midnight hours. Also abrupt drift reversals from northward to southward sometimes occurred in the course of strong and high-pitch scintillations, accompanied by sharp increases in the total electron content. These spaced-receiver measurements also established that the major axes of the diffraction pattern ellipses were oriented along the geomagnetic field line, thus demon-

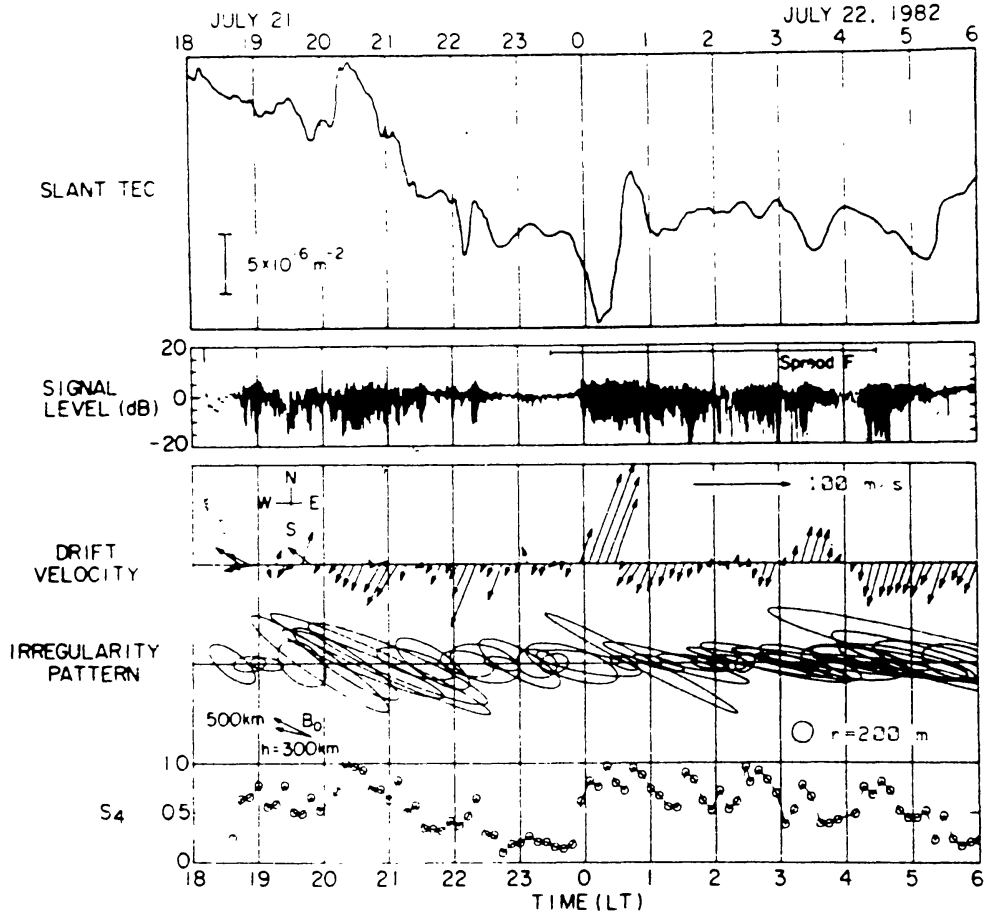


Fig. 7. Time evolution of a scintillation event recorded at Hiraiso (geomagnetic 26.3° N, 206.8°) on 21–22 July, 1982. From top to bottom, time variations in total electron content (TEC) along the radio propagation path, 136 MHz scintillation signal level, two-dimensional drift velocity vector (every 8 min), ellipse representing ground diffraction pattern (every 16 min) and $S_4$ index (every 8 min) are shown. A horizontal bar in the second panel indicates occurrence of spread-$F$ at Kokubunji (Kumagai and Ogawa, 1986).

strating the field-aligned nature of the irregularities. Another important result was that with increasing $S_4$ the minor radius decreases and the axial ratio increases. Some of these results are summarized in Figure 7.

In order to interpret these observational results in terms of irregularity characteristics, the spatial correlation function for intensity scintillations was computed by solving the fourth moment equation under the assumption of 'frozen' irregularities (Kumagai, 1987). Further a power-law form for the three-dimensional irregularity slab thickness on the results was studied. In agreement with observations, the transverse correlation distance was found to decrease with increasing $S_4$ as a result of multiple scattering (Yeh *et al.*, 1975). However, the exact variation of the transverse correlation distance with $S_4$ depends on the value of the spectral index $p$, and discrepancies between observations and computed values could be attributed, in part at least, to variations in the value of $p$ (Kumagai, 1987). Comparisons of experimental results with numerical computations also lead to an estimate of the height of the irregularity layer, which was placed in the $F$-region. For an assumed thickness of the layer, the r.m.s. electron density fluctuation required to produce scintillations of the observed strength could also be estimated from such a comparison.

### 4.2.3. *Low-latitudes*

In the vicinity of the dip equator, the geometry of spaced receiver scintillation measurements, by two antennas placed along an east–west straight line, becomes particularly simple in view of the geomagnetic field-aligned nature of the ionospheric irregularities. A simple geometry makes it possible to study the effect of 'non-frozen' behavior of ionospheric irregularities on the space-time correlation function of amplitude or intensity scintillations.

The form of a time-dependent irregularity power spectrum, for the situation where random fluctuations in the irregularity drift velocity give rise to decay (Shkarofsky, 1968) is given in (2.22). Incorporating this form in the phase screen theory of weak scintillations for a plane wave incident normally on the screen, Wernik and Liu (1983) derived a closed-form expression for the normalized space-time correlation function $R_x(x, t)$ for log amplitude $x$ from (2.23):

$$R_x(x,t) = \left\{ \mathrm{Re}\left[ (\eta - i)^{(p-2)/2} e^{-\xi/(\eta - i)} \, {}_1F_1\left( \frac{p-1}{2}, \frac{1}{2}; \frac{\xi}{\eta - i} \right) \right] - \right.$$

$$\left. - \eta^{(p-2)/2} e^{-\xi/\eta} \, {}_1F_1\left( \frac{p-1}{2}, \frac{1}{2}; \frac{\xi}{\eta} \right) \right\} \Big/ \cos\left[ \frac{\pi(p-2)}{4} \right], \quad (4.1)$$

where $\eta = \sigma_V^2 t^2 k / 2z_R$, $\xi = (x - V_{0x}t)^2 k / 4z_R$ and $p$ is the spectral index for a three-dimensional power-law irregularity spectrum of the form $\Phi_{\Delta N}(\mathbf{q}) \propto q^{-p}$. Here $x$ is along the east–west direction, $V_{0x}$ is the average irregularity drift speed along the $x$-direction, and $\sigma_V$ is the standard deviation of fluctuations in drift velocity around the mean $V_{0x}$. It has been assumed that there is no density variation in the phase-screen along the

$y$-direction which coincides with the orientation of the geomagnetic field. The changes brought about by velocity fluctuations, in the auto- and cross-correlation functions of weak scintillations, recorded by two receivers with a separation $x = 366$ m in the east–west direction, are shown in Figures 8 and 9. It is seen that velocity fluctuations

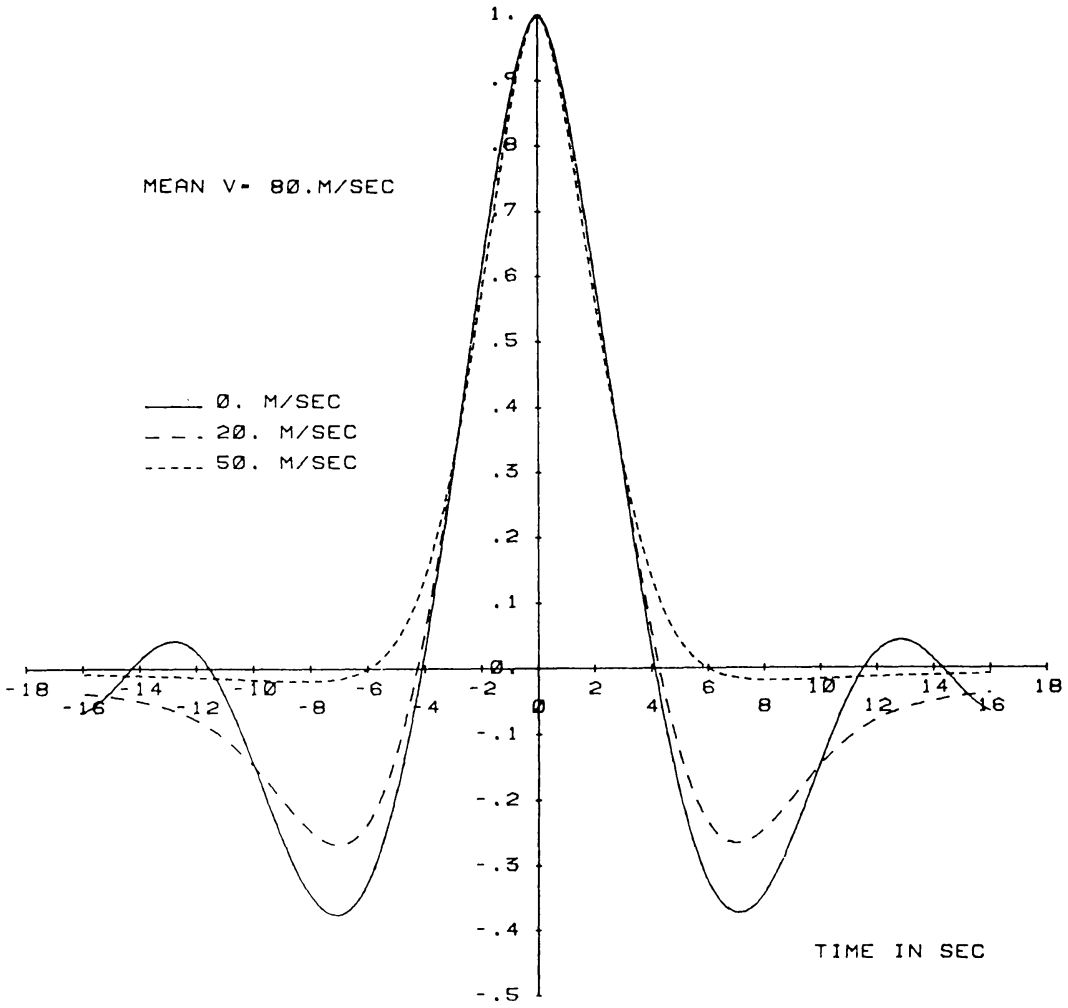


Fig. 8. Autocorrelation functions for log-amplitude, $R_\chi(0, t)$, in a model with a normal velocity distribution corresponding to three values of $\sigma_v$ (Wernik *et al.*, 1983).

mainly affect the wings of the auto-correlation function, where oscillations caused by the Fresnel filter function, discussed in Section 2, are smoothed out. This effect cannot be clearly identified in observations. The cross-correlation fucntion, however, exhibits much more drastic changes which can be easily discerned from observations. The two major effects are: (1) decorrelation due to velocity fluctuations, as expected from any temporal variation of the irregularities during the time it takes for the diffraction pattern to move from one receiver to the other; (2) a shift of the peak of the cross-correlation function towards a smaller time lag, which would lead to an overestimate of the average drift speed of the irregularities if it is simply calculated by dividing the receiver separation by the time lag for maximum cross-correlation.

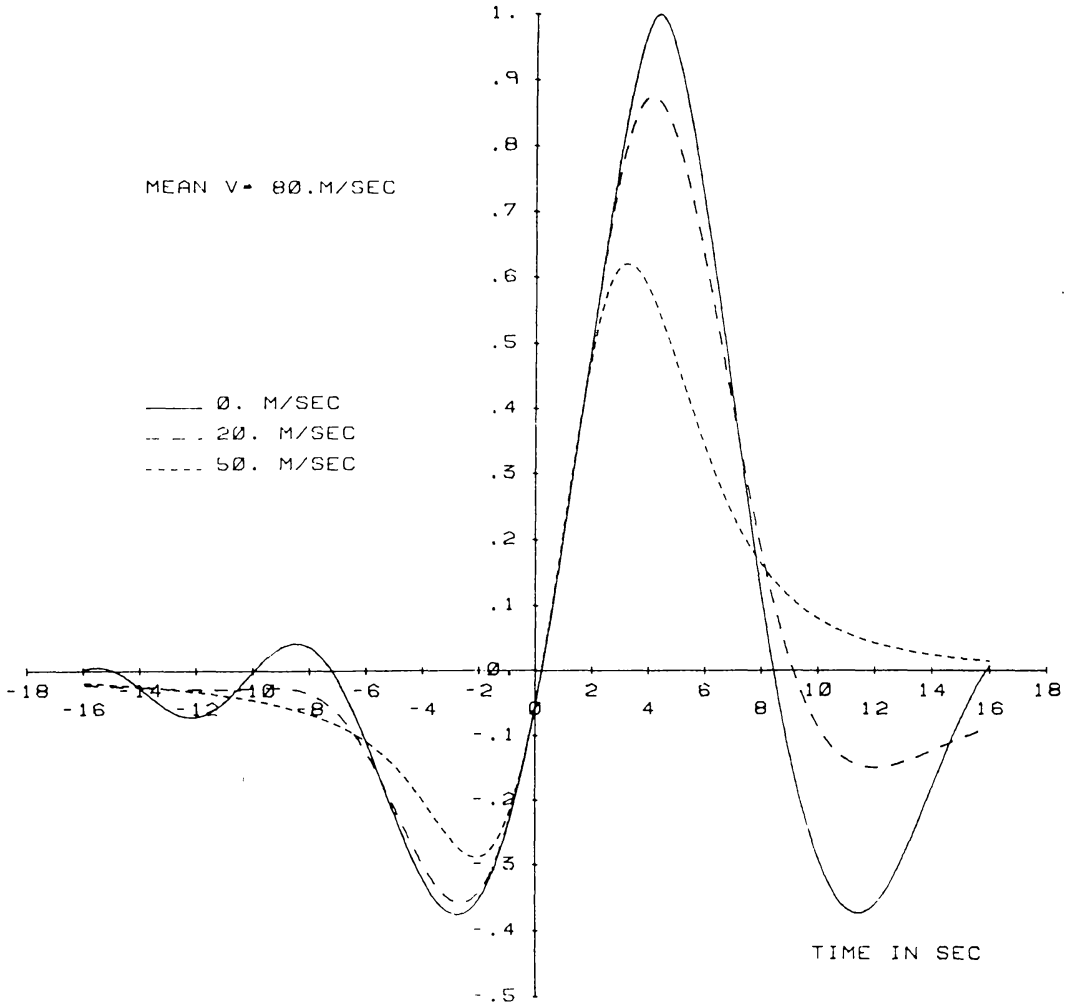


Fig. 9. Normalized cross-correlation function $R_\chi(x, t)$ for a receiver separation $x$ = 366 m, in a model with a normal velocity distribution corresponding to three values of $\sigma_v$ (Wernik *et al.*, 1983).

Auto- and cross-correlation functions computed from weak scintillation data for a 249-MHz signal, recorded at the equatorial station Ancon by three spaced receivers aligned in the east–west direction, are shown in Figure 10 (Wernik and Liu, 1983). The computed correlation functions display features expected from the expression (4.1). Wernik and Liu (1983) also considered the case of linear variation of the irregularity drift velocity along the propagation path and obtained an expression for the normalized correlation function $R_x(x, t)$. Using appropriate values of various irregularity parameters appearing in this expression, measured auto- and cross-correlation functions were compared with the model values as depicted in Figure 11. Correlation functions computed from amplitude scintillations, which were recorded at the equatorial station Guam, by two receivers placed along an east–west line with a separation of 457 m, were also modeled using (4.1) (Vacchione *et al.*, 1987). The four unknowns in the expression (4.1) for $R_x(x, t)$ are $V_{0x}$, $\sigma_V$, $p$, and $z_R$. These parameters can be estimated by a nonlinear least-squares fit of the computed correlation function by (4.1). Such a procedure, however, requires a large amount of computer time. Therefore, for the Guam

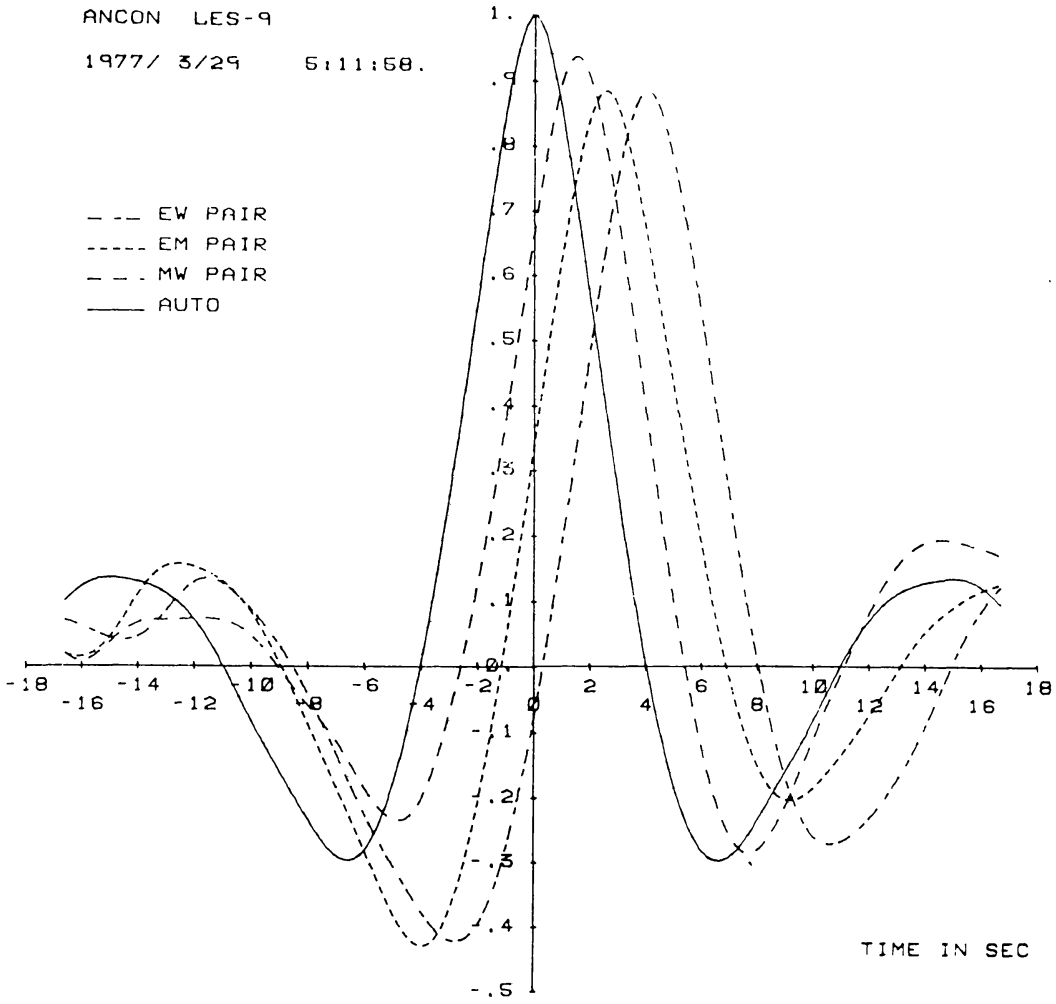


Fig. 10. Auto- and cross-correlation functions computed from amplitude scintillations on a 249 MHz signal, transmitted from LES 9 satellite and recorded at Ancon (11.71° S, 77.15° W) by three receivers aligned in the east–west direction (Wernik *et al.*, 1983).

data, the slant distance $z_R$ was independently estimated to be about 500 km, and the other parameters were determined by fitting the computed correlation functions with (4.1) (Vacchione *et al.*, 1987). A major limitation of this method of deducing $\sigma_V$ and $V_{0x}$ from spaced receiver data is that (4.1) is applicable only to weak scintillations. In this respect, there are no constraints on correlation analysis (Briggs, 1968).

Parameters which can, in principle, be derived from a correlation analysis of spaced-receiver data are: the magnitude and direction of the average drift velocity, the spatial scales and orientation of the principal axis of the observed pattern, and a measure of random temporal changes in the pattern. Recourse has to be taken to a theoretical description of the observed scintillations in order to relate these features of the observed pattern to characteristics of ionospheric irregularities. As discussed earlier, in high and mid-latitudes, random temporal changes in the pattern have been ignored and efforts have been concentrated on estimating spatial scales and orientation of the major axis, and the magnitude and direction of the drift velocity. In order to obtain a measure of

random temporal changes in the ground diffraction pattern, from scintillation records of two receivers separated by a distance $\Delta x$, as in the Ancon experiment (Wernik and Liu, 1983), it is assumed that the amplitude cross-correlation function has the following functional form (Briggs, 1968):

$$B(\Delta x, t) = f[(\Delta x - V_{0x}t)^2 + V_c^2 t^2] \,. \tag{4.2}$$

Here the characteristic random velocity $V_c$ is a measure of random changes in the pattern. If $t_m$ is the time lag for which the cross-correlation function has maximum value, then, in the presence of random changes, the apparent drift speed of the pattern is given by

$$\Delta x/t_m = V_{0x} + V_c^2/V_{0x} \,. \tag{4.3}$$

For the situation where random changes arise due to velocity fluctuations, the expression (2.23) for $B_x(x, t)$ given by Wernik *et al.* (1983) can be used to determine $t_m$ in the case of weak scintillations. Under the assumption that $\sigma_V/V_{0x} \ll 1$, the following relationship can be derived for two-dimensional irregularities:

$$\Delta x/t_m = V_{0x} + \sigma_V^2/V_{0x} \,. \tag{4.4}$$

This at once leads to the identification, for weak scintillations, of $V_c$ with $\sigma_V$ (Wernik *et al.*, 1983; Vacchione *et al.*, 1987).

One of the methods, based on assumption (4.2), which was found to be useful in determining $V_c$ from spaced receiver data was the 'peak-value' method (Vacchione *et al.*, 1987). According to this, the true drift $V_0$ of the irregularities and $V_c$ are given by:

$$V_0 = \Delta x t_m/(t_m^2 + t_p^2) \,, \tag{4.5}$$

$$V_c^2 = \Delta x V_0/t_m - V_0^2 \,, \tag{4.6}$$

where $t_p$ is the time lag for which the auto-correlation of amplitude equals the peak value of the cross-correlation function for amplitudes recorded by two receivers separated by a distance $\Delta x$. Values of average drift $V_0$ and the characteristic random velocity, $V_c$, have been computed from spaced receiver observations of nighttime scintillations on a VHF signal, at the equatorial station Guam, using this method and some variations of it (Spatz *et al.*, 1988). Whereas the average drift, $V_0$, of the pattern observed on ground can be identified with the average drift of the irregularities even when strong scintillations are observed, the relationship between $V_c$ and irregularity characteristics becomes complicated under these conditions. For strong scintillations, it is necessary to obtain the space-time correlation function for intensity from a solution of the fourth moment equation, in order to relate $V_c$ to certain irregularity characteristics.

An average drift velocity of 120 to 150 m $s^{-1}$ was obtained for most of the nighttime scintillation events studied by Spatz *et al.* (1988). The drift velocities were found to decrease gradually after 21:00 LT. Due to the orientation of the signal paths to the receivers at Guam, this average drift can, in general, have contributions from both a

zonal drift $V_E$ and a vertical drift $V_n$ of the irregularities:

$$V_0 = V_E - V_n \tan\theta \sin\phi, \tag{4.7}$$

where $\theta$ is the zenith angle, and $\phi$ is the azimuth of the signal path measured from the magnetic meridian. Dynamics of ionospheric plasma turbulence in the equatorial region have also been studied using a radar interferometer technique which was introduced by Farley *et al.* (1981) at the Jicamarca Radio Observatory. During the Project Condor equatorial spread *F* campaign, spaced receiver scintillation observations were carried out alongside radar interferometer measurements. Analysis of data for short intervals on two nights yielded spaced receiver drifts which were 10–20% higher than simultaneous measurements by radar interferometer (Basu *et al.*, 1986). These results are expected to differ because whereas scintillation data have maximum contribution from a region in the vicinity of peak ionization density, the radar interferometer may be tracking irregularities in a different altitude range. The characteristic velocity derived from spaced receiver data was found to decline sharply in a short period following the onset of scintillations in the post-sunset hours (Vacchione *et al.*, 1987; Spatz *et al.*, 1988).

Spaced receiver scintillation data from Guam was also used to compare the behavior

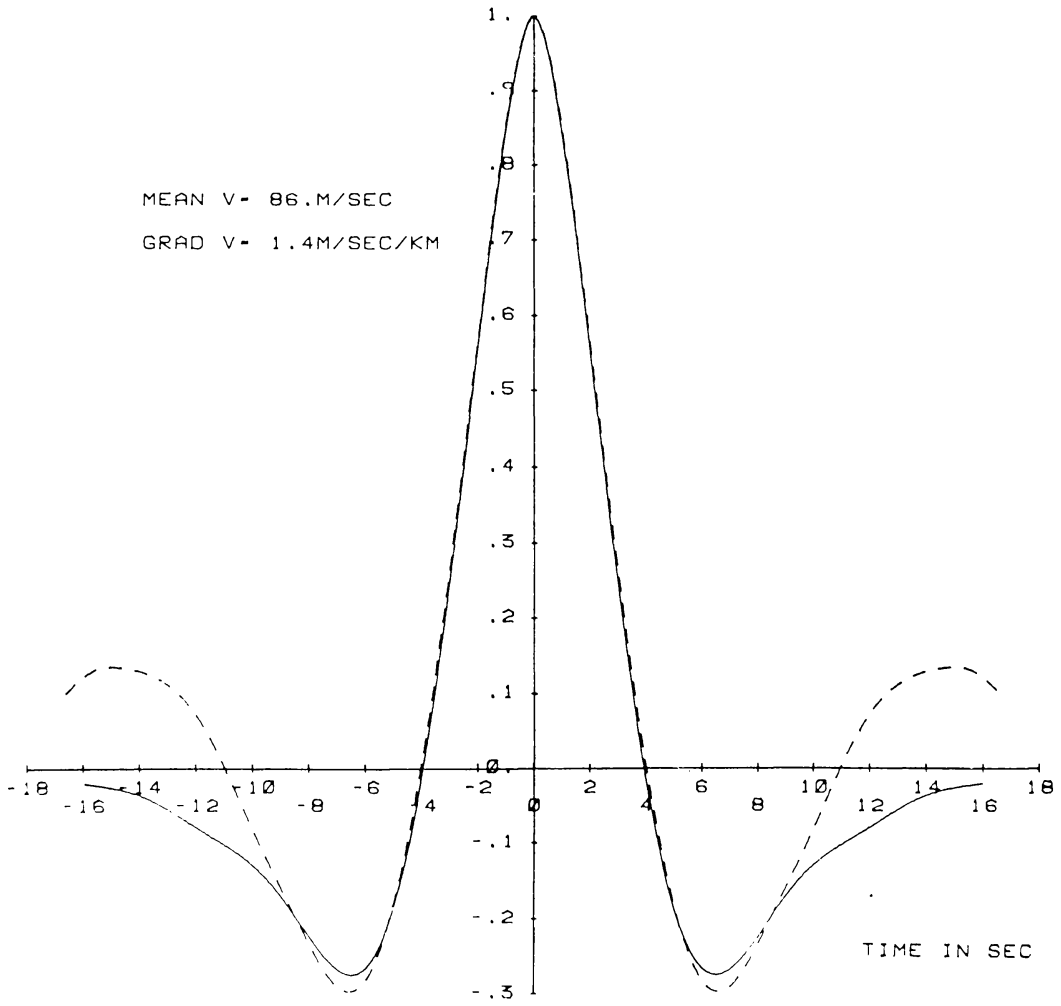

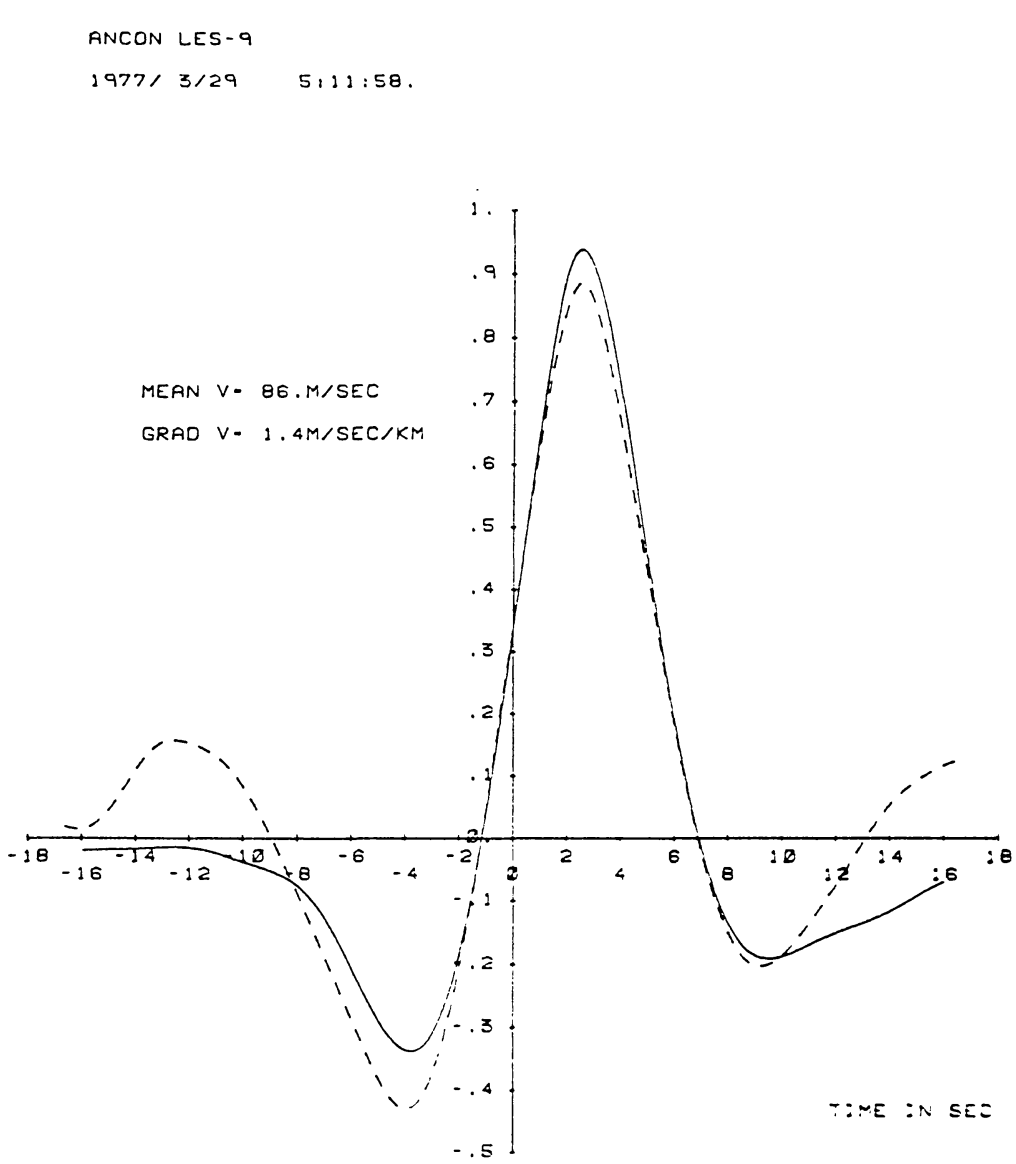


Fig. 11. (a) Comparison between the measured (dashed line) and modeled (solid line) correlation function for receivers separated by 244 m. In the model, the irregularity drift velocity is taken to vary linearly along the propagation path. (b) Same as (a) for cross-correlation functions (Wernik *et al.*, 1983).

of the average drift $V_0$ with local time under geomagnetically quiet and disturbed conditions (Bhattacharyya *et al.*, 1989). A composite plot of $V_0$ computed for nine nighttime scintillation events which occurred during geomagnetically quiet periods around summer solstice and equinox is shown in Figure 12(a). On rare occasions, $V_0$ is seen to be negative in the early evening hours, which, according to (4.7), implies either a westward drift or a large upward drift of the irregularities. Either or both of these conditions may be sometimes present during early evening hours. The observed local time behavior of the average drift is similar to that deduced from radar measurements of equatorial *F*-region zonal plasma drifts (Fejer *et al.*, 1985). Variation of $V_0$ with local time, obtained from spaced receiver data of seven magnetically disturbed days with $\Sigma k_p \geq 30$, is shown in Figure 12(b). There is a distinctly greater occurrence of negative

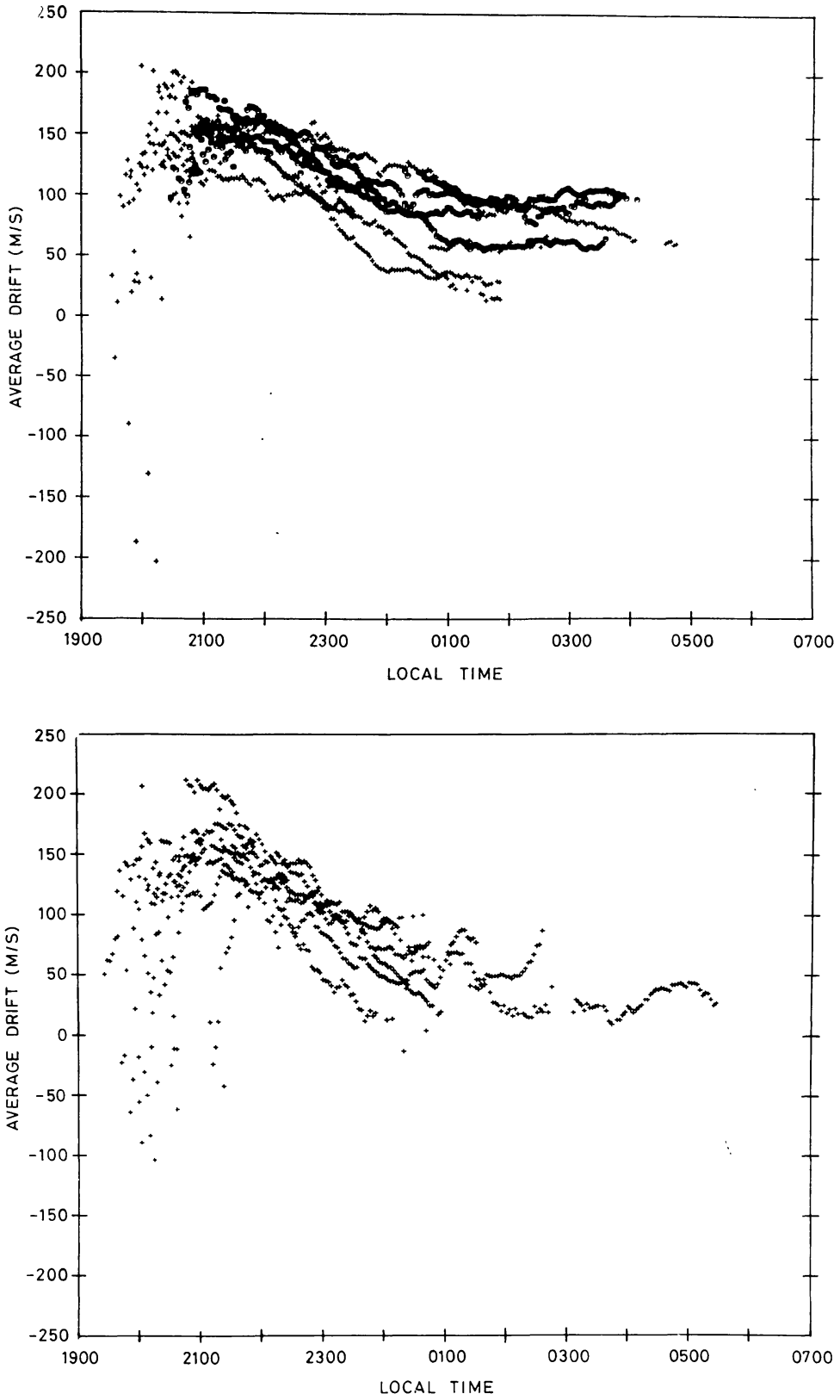


Fig. 12. (a) Local time variation of the averate drift of equatorial *F*-region irregularities obtained from spaced receiver measurements of scintillations at Guam (magnetic dip 4.8° N) for some magnetically quiet periods during summer solstice (crosses) and equinox (circles). (b) Same as (a) for seven magnetically disturbed days with $\Sigma K_p \geq 30$ (Bhattacharyya *et al.*, 1989).

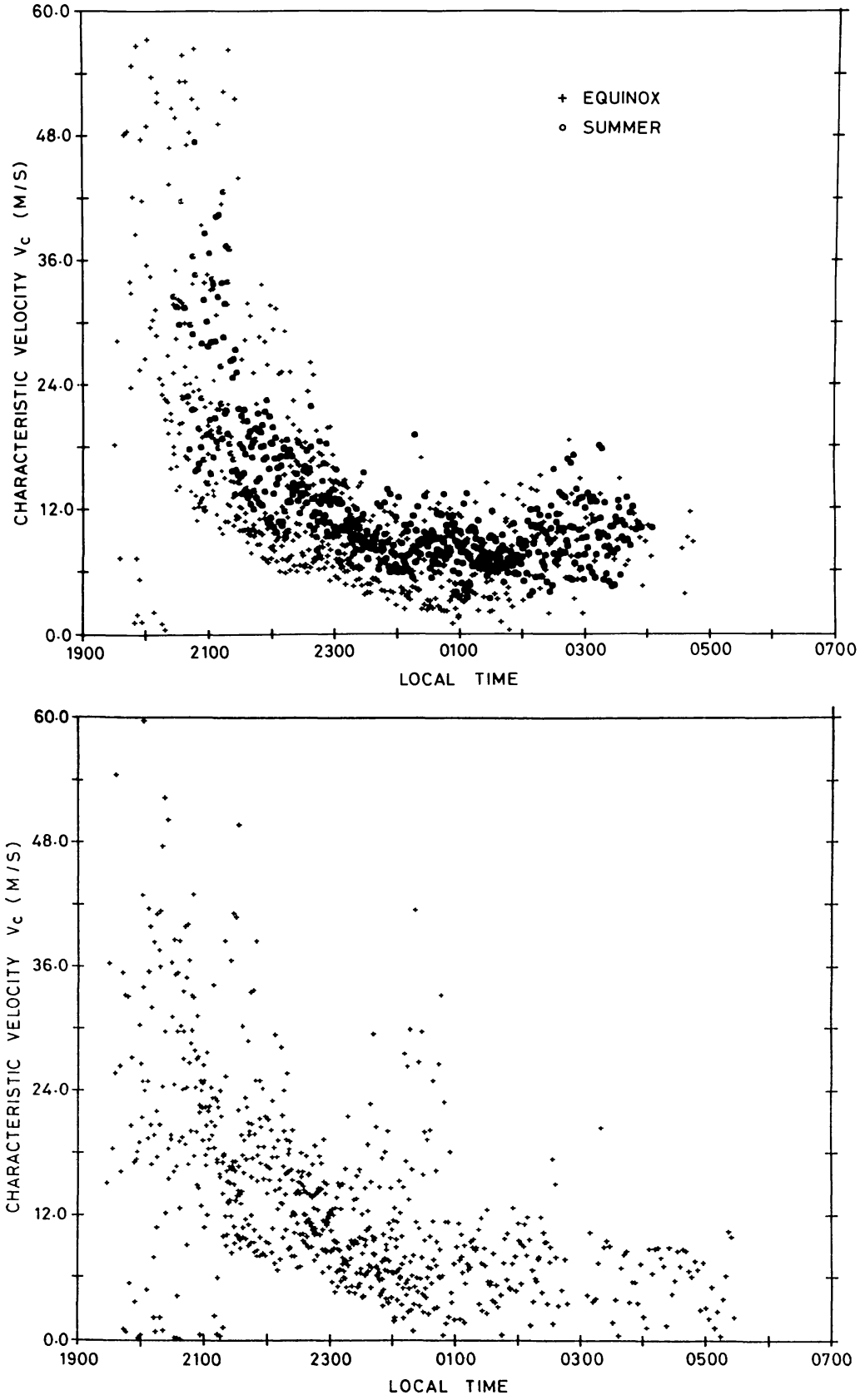


Fig. 13. (a) Local time variation of the characteristic velocity obtained from spaced-receiver scintillation measurements at Guam for the magnetically quiet periods shown in Figure 12(a). (b) Same as (a) for the magnetically disturbed days shown in Figure 12(b) (Bhattacharyya *et al.*, 1989).

drift in the early evening hours for these days compared to the quiet days. Apart from this, the tendency of $V_0$ to decrease beyond 21:00 LT still persists.

For geomagetically quiet periods, changes in $V_c$ with local time were found to follow the same pattern both during equinox and summer solstice as shown in Figure 13(a). There is a shift in time between the two due to the later onset of scintillations during summer on account of delayed sunset. In the post-midnight period, a gradual increase of $V_c$ is discernible, with $V_c$ acquiring a minimum value around 01:00 LT. For the winter season, lack of sufficient data precluded the emergence of a definite pattern. For magnetically disturbed days, $V_c$, depicted in Figure 13(b), is seen to occasionally have higher values than expected around midnight, but the characteristic steep decline in the premidnight period still exists (Bhattacharyya *et al.*, 1989).

It is necessary to relate $V_c$ derived from the observed scintillation pattern to some physical properties of ionospheric irregularities before the local time variation of $V_c$ can be given a geophysical interpretation. Towards this end, the space-time correlation function for intensity was obtained by solving the fourth moment equation for an irregularity power spectrum of the form (2.22), as discussed in Section 2. Local time variation of the spectral index associated with a power-law irregularity spectrum,

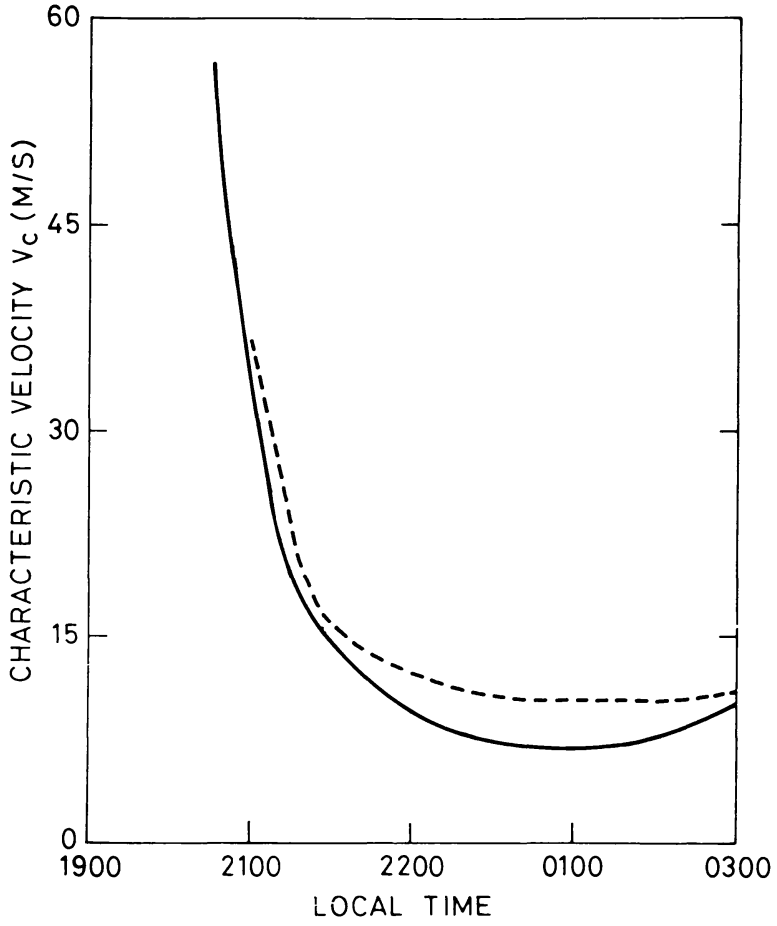


Fig. 14. Variation of measured characteristic velocity ($V_c$) with local time (solid line) and estimate of the variation of $\sigma_v$ with local time (dotted line) (Bhattacharyya *et al.*, 1989).

derived by Spatz *et al.* (1988) from weak amplitude scintillations recorded at Guam, was used in the numerical computation of $V_c/\sigma_V$ for different values of the $S_4$-index, at different local times. On the basis of this calculation, an approximate pattern for the variation of $\sigma_V$ with local time is depicted in Figure 14 (Bhattacharyya *et al.*, 1989). It is seen that $\sigma_V$ also declines steeply in a short time after 21:00 LT. A possible explanation put forth for this behavior attributes the velocity fluctuations to electric field fluctuations associated with the generalized Rayleigh–Taylor instability, which is generally believed to give rise to the equatorial *F*-region irregularities (Haerendel, 1974; Zargham and Seyler, 1987). Variability of the zonal drift of equatorial *F*-region irregularities has been studied using the radar interferometer technique (Kudeki and Franke, 1986). Fluctuations in the zonal drift with amplitudes estimated to be as high as 30% and with time-scales of several minutes have been detected at Jicamarca between 21:00 and 22:00 LT. These radar interferometer observations also indicated that velocity fluctuations observed near the *F*-region peak could be associated with density irregularities having horizontal scale sizes $\gtrsim 1$ km, and could, therefore, cause decorrelation of forward scattered VHF signals monitored by spaced receivers.

### 4.3. Mutual coherence function

Even before a multiple scatter theory was developed for describing strong scintillations, it was realized that the mutual coherence function (MCF) is independent of the Fresnel parameter $\lambda z/4\pi$, and that it is invariant under free-space propagation (Booker *et al.*, 1950). This last property of the MCF is easily seen to be a consequence of (2.35), where (2.36) ensures the first one. Examples of weak amplitude and phase scintillation spectra presented earlier, clearly demonstrate that the Fresnel dimension plays a major role in determining their structure. This aspect has been exploited to determine either the transverse drift speed of the irregularities or the effective height of the irregularity layer, but no information could be obtained about certain other parameters such as the outer scale associated with the irregularity structure. On the other hand, the MCF, being independent of the Fresnel dimension, can provide information about the irregularities even when the effective height of the irregularity layer ($z$) is unknown. Also, as pointed out in section 2.4, a closed form expression exists for the MCF which is valid in the multiple scatter regime as well. With the availability of phase coherent signals, transmitted from satellites, it became possible to compute the MCF for transionospheric radio waves.

The first such measurements for transionospheric radio waves used Wideband satellite data (Rino and Owen, 1982). Using a three-dimensional irregularity spectral density function of the form $\Phi_{\Delta N}(\mathbf{q}) = C_s q^{-(2\nu+1)}$, these authors obtained an expression for the MCF which is valid for separations $\xi$ (see (2.36)) that lie between the outer and inner scale cutoffs. The measured MCF's were found to be in agreement with this expression for small values of the separation parameter. For large values of the separation parameter, the measured MCF's can be unreliable due to lack of stationarity in data caused by inhomogeneous large-scale phase variations. Thus, detrending of the data before the computation of MCF is of paramount importance.

In this context, it becomes necessary to justify the use of (2.36) to describe the MCF derived from detrended scintillation data. Bhattacharyya and Rastogi (1991) have demonstrated that the theoretical derivation of MCF retains its validity if a suitable criterion is established for eliminating large scale trends from the data. If the ionospheric irregularities are assumed to be 'frozen', $A_{\Delta N}(\xi, \tau)$ appearing in (2.36) can be written in terms of the three-dimensional irregularity power spectrum $\Phi_{\Delta N}(\mathbf{q})$:

$$A_{\Delta N}(\xi, \tau) = 2\pi \int_{-\infty}^{\infty}\int \Phi_{\Delta N}(\mathbf{q}_\perp, 0)\, e^{i\mathbf{q}_\perp \cdot (\xi - \mathbf{V}\tau)}\, d\mathbf{q}_\perp \,. \tag{4.8}$$

In a model of anisotropic irregularities, in the special case where the direction of propagation ($z$-axis) is normal to the elongation axis ($y$-axis) which is along the geomagnetic field, $\Phi_{\Delta N}(\mathbf{q}_\perp, 0)$ has the form

$$\Phi_{\Delta N}(\mathbf{q}_\perp, 0) \propto \left[1 + \frac{q_x^2 + \eta^2 q_y^2}{q_0^2}\right]^{-p/2}, \tag{4.9}$$

where $\eta$ is the anisotropy factor, and $q_0$ is the outer scale wave number for scale sizes in the $x$-direction. If the irregularity drift velocity is in the $x - z$ plane and has a component $V_0$ transverse to the signal path, $A_{\Delta N}(0, \tau)$ is given by

$$A_{\Delta N}(0, \tau) = \frac{8\sqrt{\pi}}{2^{p/2}} \frac{1}{q_0} \frac{\langle (\Delta N)^2 \rangle}{\Gamma[(p-3)/2]} K_{p/2-1}(|q_0 V_0 \tau|)\, (|q_0 V_0 \tau|)^{p/2-1} \,. \tag{4.10}$$

This form of $A_{\Delta N}(0, \tau)$ was used in (2.36) to obtain the MCF, $\Gamma_2(0, z_R, \tau)$, which could be compared with the MCF derived from amplitude and phase scintillation data recorded by a single receiver located at a distance $z_R$ from the top of the irregularity layer. This expression for $\Gamma_2(0, z_R, \tau)$ is of course independent of $z_R$ as discussed earlier but depends on various other parameters of the irregularities including the power spectral index $p$, the transverse drift speed $V_0$ and the outer scale wave number $q_0$, the last two parameters occurring in the combination $q_0 V_0$. In fact, the shape of $\Gamma_2(0, z_R, \tau)$ is determined essentially by $q_0 V_0$ and another parameter which is basically a measure of the strength of the irregularities. The function $f(t)$ defined by

$$f(t) = -\ln[\Gamma_2(0, z_R, t)/\Gamma_2(0, z_R, 0)] \,, \tag{4.11}$$

which is half of the structure function for phase fluctuations imposed on the incident wave by the irregularity slab, has been computed from equatorial nighttime scintillation data (Bhattacharyya and Rastogi, 1991). Some examples of computed $f(t)$ together with theoretically fitted curves are shown in Figures 15 and 16. Theoretically, $f(t)$ should initially increase with time starting from its value 0 at $t = 0$, and for sufficiently large values of $t$, $f(t)$ should approach a constant value of $r_e^2 \lambda^2 B_{\Delta N_T}(0, 0)$, where $B_{\Delta N_T}(\boldsymbol{\rho}, t)$ is the space-time correlation function for fluctuations in the total electron content along the signal path defined by (2.4). The product $q_0 V_0$ determines how rapidly $f(t)$

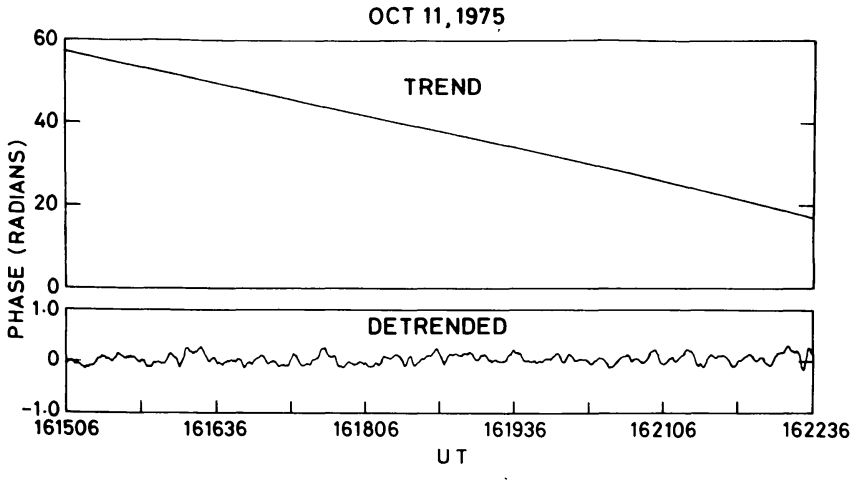


(a)

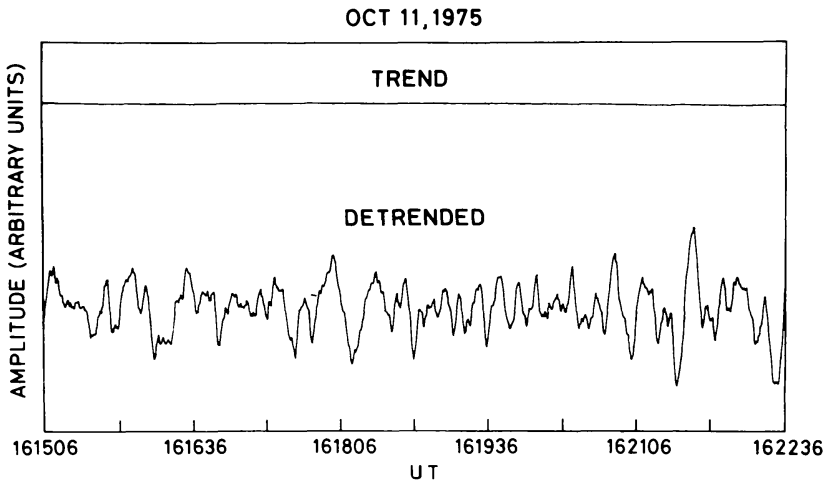


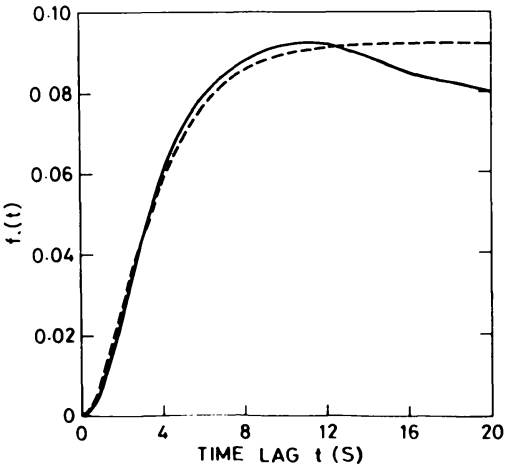


(b)

Fig. 15. (a) Phase trend, filtered phase, amplitude trend and filtered amplitude for a 140-MHz signal from the geostationary satellite ATS 6 received at the equatorial station Ootacamund during a period of weak to moderate scintillations ($S_4 = 0.48$). (b) $f(t)$, which is related to the MCF through Equation (4.11), computed from data (solid line) and from theory (dashed line) (Bhattacharyya and Rastogi, 1991).

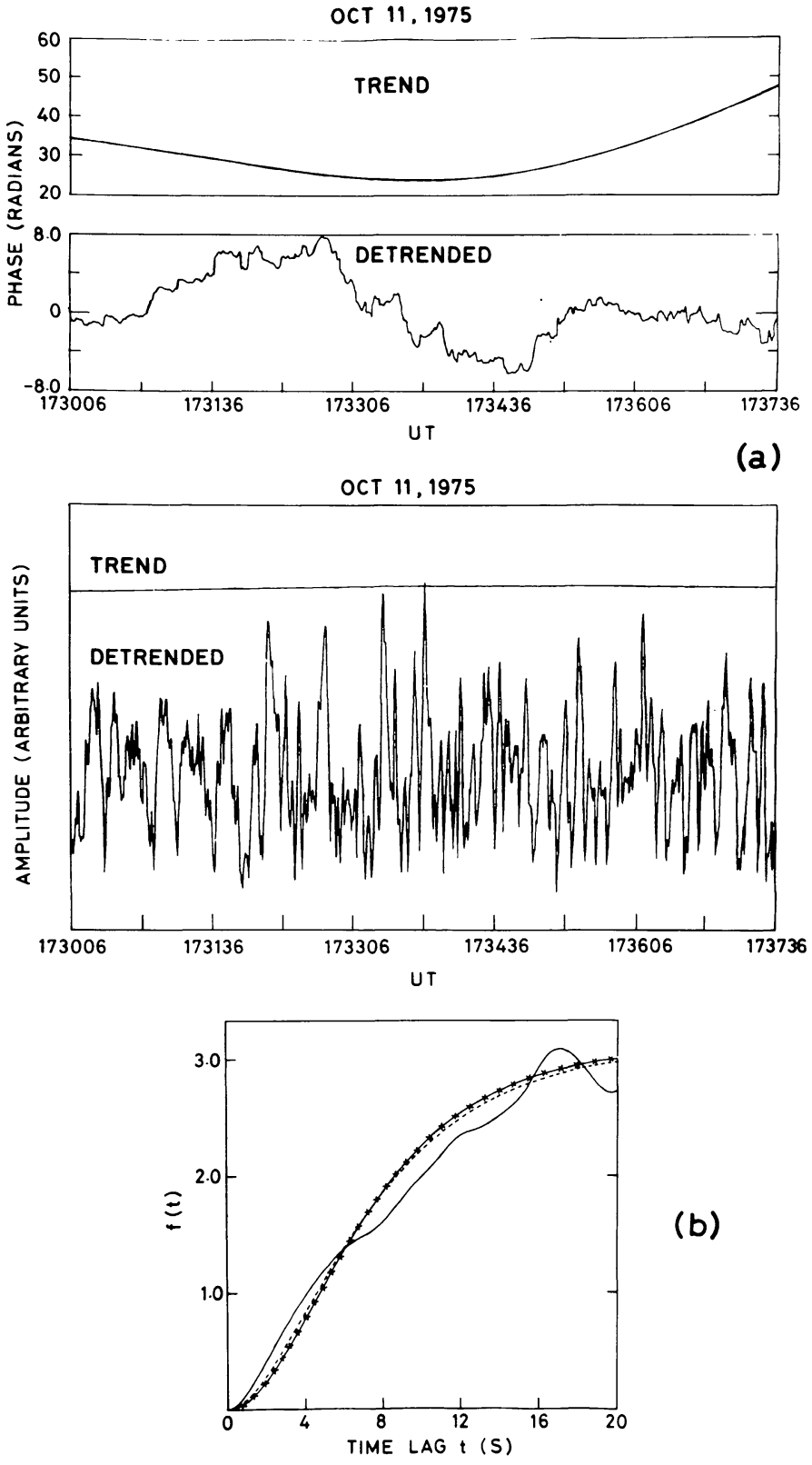


Fig. 16. (a) Same as Figure 15(a) during a later period when scintillations are strong ($S_4 = 0.90$). (b) Same as Figure 15(b) for the data shown in Figure 16(a). The crossed line is the theoretical $f(t)$ for $p = 6$, and the dashed line is for $p = 5$. The theoretical fits are obtained with a value of $\langle(\Delta N)\rangle^{1/2}$ which is almost thrice as large as that required for the theoretical fit in Figure 15(b). The scale length $L_0$ ( $= 2\pi/q_0$) is to found to be about twice that found for Figure 15(b) (Bhattacharyya and Rastogi, 1991).

approaches its maximum value. Hence, with a reasonable estimate of $V_0$, it is possible to deduce $q_0$ from the shape of $f(t)$ deduced from observations. Further, the theoretical $f(t)$ is not very sensitive to variations in the spectral index $p$. Although, equatorial $F$-region irregularities sometimes display a two-component power-law spectrum, a single-component power-law spectrum with a high spectral index, which is derived for shorter wavelength irregularities, from scintillation spectra, is found to be adequate for reproducing the short time-scale behavior of $f(t)$. The transverse drift $V_0$ estimated from the power spectra of weak scintillation data, as described in Section 4.1, can be used to determine $q_0$, once $q_0 V_0$ has been deduced from $f(t)$. However, the $q_0$ thus determined actually corresponds to the 'intermediate break scale' $L_0$, at which the irregularity power spectrum changes from a shallow to a steep spectral index. The root mean-square density fluctuation in the irregularity slab can also be estimated from the computed $f(t)$ (Bhattacharyya and Rastogi, 1991).

## 5. Conclusion

In this paper, methods used to extract information about ionospheric irregularities, from measurements of scintillations on transionospheric signals, have been reviewed. The emphasis has been on results obtained since the mid seventies, as earlier observations and theoretical developments have been discussed extensively in a number of review papers (Crane, 1977; Aarons, 1977, 1982; Basu and Kelley, 1979; Yeh and Liu, 1982; Basu and Basu, 1985).

In the theoretical arena, the last fifteen years have seen much progress in the understanding of strong scintillations. Since a large fraction of scintillation data falls in the category of strong scintillations, it became imperative to devise ways of handling the multiple scatter regime. Extension of the phase screen approximation to strong scatter conditions (Rumsey, 1974; Marians, 1975; Rino, 1979) yielded important results for the dependence of the $S_4$-index on irregularity strength and the behavior of the intensity correlation function and its power spectrum when the irregularities are considered to be 'frozen'. It became clear that irregularities of scale sizes greater than the Fresnel dimension contribute to small-scale fluctuations in amplitude when the scintillations are strong (Booker and Majidi Ahi, 1981) thereby destroying the one-to-one correspondence between irregularity scale lengths and scale sizes associated with the pattern observed on the ground. Questions were raised, however, about the validity of these results, based on the phase screen approximation, when the incident wave underwent multiple scattering within a thick layer of irregularities. The answer was sought from the solutions of the equations satisfied by the moments of the complex amplitude of the wave field. Of the various moments which can be directly related to statistical parameters computed from amplitude and phase scintillation data, only the mutual coherence function $\Gamma_2 = \langle u(z, \boldsymbol{\rho}, t) u^*(z, \boldsymbol{\rho}', t') \rangle$ has an analytic solution in terms of the structure function for phase fluctuations imposed by the irregularity slab (Yeh and Liu, 1982; Rino and Owen, 1982). The fourth moment $\Gamma_4$, which is of special importance as it yields the $S_4$-index as well as the intensity correlation function, has to be obtained by numeri-

cally solving the equation satisfied by it. Such computations have demonstrated the decorrelation caused by multiple scattering, in agreement with observations (Yeh *et al.*, 1975). Numerical solutions of the fourth moment equation for an extended irregular medium were also compared with results obtained from the phase screen approximation and the latter was found to provide a fairly accurate description of the irregularity layer for the purpose of the computation of $S_4$-index and intensity correlation function (Booker *et al.*, 1985).

Another area where rapid strides have been made in recent years is the theoretical study of the effect of 'non-frozen' behavior of ionospheric irregularities on the observed scintillations. In the first effort in this direction, statistical characterization of spatial as well as temporal variations in ionospheric plasma density were incorporated in the phase screen theory of weak scintillations (Wernik *et al.*, 1983). A description of non-frozen turbulent medium given by Shkarofsky (1968) was used for the situation where decay of the irregularities is caused by either drift velocity fluctuations or diffusion. The effect of a regular variation of velocity inside the turbulent layer was also studied by Wernik *et al.* (1983). It was found that temporal variation of ionospheric irregularities, attributed to these causes, produces significant changes in the cross-correlation function of amplitudes recorded by spaced receivers monitoring the incident wave. Computation of the space-time intensity correlation function for scintillations caused by either a deep random phase screen (Franke, 1987) or a thick layer of irregularities (Bhattacharyya *et al.*, 1989), demonstrated that the changes due to 'non-frozen' behavior of the irregularities occur in the case of strong scintillations as well. These calculations set the stage for proper interpretation of spaced-receiver scintillation measurements.

With a better theoretical understanding of strong scintillations, multifrequency observations of scintillations could be put to greater use in the extraction of irregularity characteristics. For instance, comparison of modeling results based on numerical simulation of a phase screen, with observations of multifrequency VHF and GHZ amplitude scintillations in the equatorial region, yielded a picture of equatorial *F*-region irregularities which was different from what had been obtained in earlier scintillation studies. It was found that these irregularities are sometimes characterized by a two-component power-law spectrum which has a shallow large-scale regime and a steeper small-scale regime, with the break in spectral slope occurring at an irregularity scale size around 1 km (Franke and Liu, 1983).

It was further realized that, whereas Fresnel filtration effects limit the information that can be extracted from weak amplitude scintillation data to irregularities with scale sizes $\lesssim$ the Fresnel dimension, phase scintillation data do not suffer from such restrictions. Thus power spectra of weak phase scintillations can be used directly to obtain irregularity characteristics for scale sizes larger than the Fresnel dimension as well. Such a study led to an unambiguous determination of the spectral indices and the break scale length associated with a two-component power-law spectrum for equatorial *F*-region irregularities (Bhattacharyya and Rastogi, 1986). In the nighttime auroral region, phase scintillation data revealed a multiple-regime power-law structure which could be interpreted in terms of size-dependent anisotropy of the irregularities (Fremouw *et al.*, 1985).

Another major development in scintillation studies was the analysis of spaced-receiver scintillation data to estimate the anisotropy of irregularities (Rino *et al.*, 1978; Rino and Livingston, 1982; Kumagai and Ogawa, 1986; Costa *et al.*, 1988) and the effect of their 'non-frozen' behavior, epitomized by the so-called characteristic random velovity $V_C$ (Wernik *et al.*, 1983; Basu *et al.*, 1986; Vacchione *et al.*, 1987; Spatz *et al.*, 1988; Bhattacharyya *et al.*, 1989). With the advances made in the theoretical computation of space-time characteristics of scintillations produced by 'non-frozen' irregularities it became possible to relate $V_C$ with some irregularity characteristic such as the standard deviation, $\sigma_V$, of fluctuations in the drift speed of the irregularities, in the situation where decay of the irregularities occurred due to such fluctuations of the irregularity drift about a mean value. The observed variation of $V_C$ with local time, which was deduced from spaced-receiver measurements of equatorial nighttime amplitude scintillations caused by *F*-region irregularities, was explained on the basis of the theoretical relationship between $V_C$ and $\sigma_V$ (Bhattacharyya *et al.*, 1989). Such a study naturally involves the physical mechanisms, such as plasma instabilities, which are responsible for the presence of scintillation-causing irregularities in the ionosphere. Growth of an instability in ionospheric plasma, in turn, brings into picture some parameters of the ambient plasma such as the prevalent density gradients, electric field, etc. Thus, measurements of ionospheric scintillation can lend support to various other ionospheric observations.

During the last decade or so, the trend in experimentation has been towards coordinated measurements of scintillations together with *in situ* and radar observations (Basu *et al.*, 1980; Rino *et al.*, 1981; Kelley *et al.*, 1986). Some of the results obtained from such experiments have been described in this review. In the equatorial region, observation of amplitude scintillations caused by BSS irregularities, which had been identified in simultaneously obtained satellite data, corroborated their sinusoidal nature as well as location (Basu *et al.*, 1986). A coordinated study of auroral zone plasma enhancements involving radar, optical, particle precipitation and scintillation measurements, yielded information about the location of the region where ionization is produced, the role of convection in the auroral *F*-region, and the relation of sub-kilometer irregularities to large-scale structures in the auroral ionosphere (Weber *et al.*, 1985). During the Project Condor equatorial spread *F* campaign, the radar interferometer technique was used to estimate the *F*-region zonal drift variability (Kudeki and Franke, 1986). The estimated standard deviations were consistent with values of $V_C$ derived from spaced receiver observations of scintillations during this campaign (Basu *et al.*, 1986) thus lending credence to the hypothesis that, temporal variation of the irregularities during the observation period was due to decay caused by fluctuations in the irregularity drift. The above examples bring out the usefulness of multi-technique observations of ionospheric irregularities.

An overall picture of ionospheric irregularities, which could emerge on the basis of information extracted from amplitude and phase scintillation data obtained in different geographic regions, has not been put together as yet. This is partly because further investigations need to be carried out in a number of areas. For instance, measurement

of scintillations by three appropriately placed receivers could be utilized to determine simultaneously the anisotropy of the irregularities as well as random temporal variations. The methodology exists (Costa *et al.*, 1988) but the computations may be cumbersome. A study of changes in irregularity parameters, in different geographical regions, during periods with varying levels of geomagnetic activity, can shed some light on the coupling between high- and low-latitude ionospheres. As far as analysis techniques are concerned, dispersion analysis of spaced receiver scintillation data (Wernik *et al.*, 1983) may yield interesting results in those situations where irregularity drifts are expected to be wavelength dependent, as in the case of electrojet irregularities (Kudeki *et al.*, 1982).

The results reviewed in this paper are mainly concerned with statistical properties of ionospheric irregularities. However, it must be borne in mind that statistical features like the irregularity power spectrum do not reveal the true nature of ionospheric turbulence. For instance, ionospheric density fluctuations characterized by sharp gradients, which imply a high degree of phase coherence of their Fourier spectral components; and a turbulent electron density structure, which has very little phase coherence in its spectral components; both can yield identical irregularity power spectrum. This was explicitly demonstrated by using equatorial *F*-region rocket data dollected over Natal, Brazil (Costa and Kelley, 1978). These authors computed the Fourier transform of the meas-

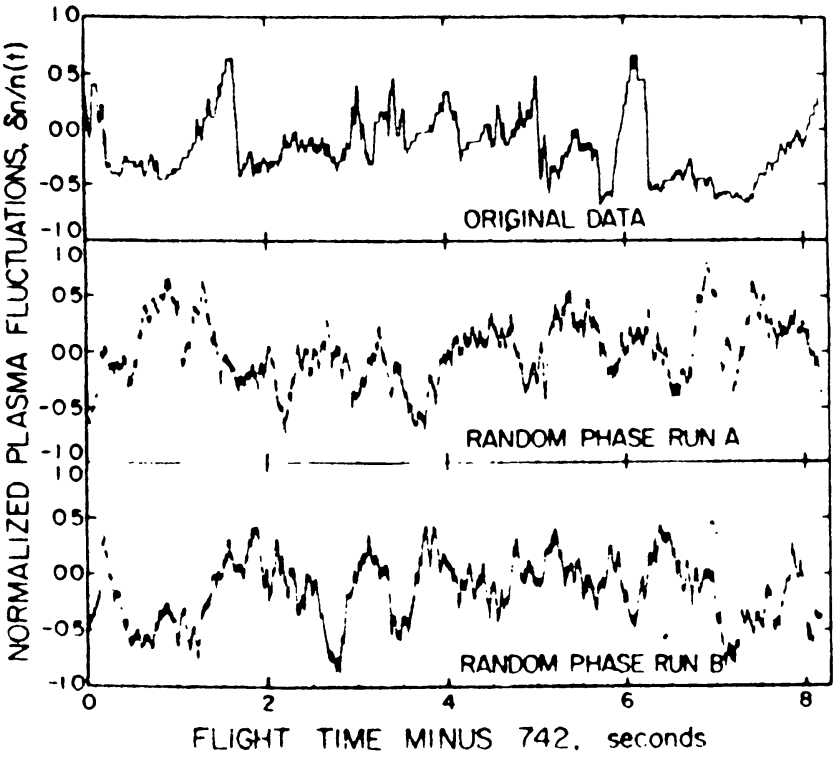


Fig. 17. The upper plot shows detrended data obtained from the downleg trajectory of a rocket launched eastward from Natal, Brazil during equatorial spread *F* conditions. The two lower plots are reconstructed time domain samples using the same data but with their Fourier coefficients multiplied by a random phase factor before reconstruction (Costa and Kelley, 1978).

ured electron density, and then added a random phase to each complex coefficient before reassembling in the time domain. The resultant density fluctuation is shown along with the original data in Figure 17. On the basis of this, it was concluded that the observed $K^{-2}$ power spectrum was not due to a turbulent cascade of wave energy which results in power law spectra for fluid turbulence, but could be attributed to a steepening of individual waves, in agreement with earlier theoretical calculations on the non-linear development of the collisional Rayleigh–Taylor (RT) instability on the bottom side (Chaturvedi and Kaw, 1975; Chaturvedi and Ossakow, 1977). Features of ionospheric scintillations produced by the two different types of density variations described above, have been studied by Wernik *et al.* (1980) by solving the relevant parabolic equation satisfied by the wave field. In the light of the above discussion, it seems natural to ask if it is possible to obtain information about the chaotic behavior of ionospheric density fluctuations from an analysis of scintillation data.

For this purpose, the ideas of deterministic chaos and strange attractors (Eckmann and Ruelle, 1985) were applied recently to nighttime amplitude and phase scintillation data collected at an equatorial location (Bhattacharyya, 1990a). The data was used to estimate a correlation exponent which provides a lower bound the 'information dimension' associated with the attractor of the system under study. This, in turn, indicates whether the turbulence represented by the signal fluctuations is described by an infinite number of degrees of freedom or whether it is deterministic, in that, it can be characterized by a few degrees of freedom. Some results obtained from the above analysis are shown in Figures 18 and 19, and lead to the conclusion that (a) ionospheric turbulence is generally low dimensional; (b) as the strength of ionospheric scintillations increases after the onset of scintillations, the 'information dimension' associated with phase scintillation data usually does not register an increase. The increased scintillations are attributed to further steepening of individual waves in the ionosphere which causes 'focusing' (Berry, 1977; Booker and Majidi Ahi, 1981) of the incident wave. This results in a higher value of the 'information dimension' derived from amplitude scintillation data. Therefore, a higher value of the $S_4$-index or of $\sigma_\phi$, the standard deviation of phase fluctuations, does not necessarily imply higher dimensional chaos in the ionosphere. In recent years, the possibility of occurrence of chaotic patterns in the temporal behavior of ionospheric density fluctuations, arising due to interchange instabilities, has been investigated (Huba *et al.*, 1985; Hassam *et al.*, 1986), but there has not been any theoretical attempt, so far, to look into chaotic spatial behavior of these density fluctuations.

In this paper we have focused our review on the effects of ionospheric irregularities to transionospheric radio propagation. There are, of course, other aspects of ionospheric irregularities currently receiving active attention by research workers but not reviewed in this paper. Among them are the following few examples.

(1) Global morphology of ionospheric irregularities and scintillation (Herman, 1966; Aarons, 1982) and their empirical modeling (Fremouw and Secan, 1984).

(2) Physical mechanisms for the production of ionospheric irregularities (Chaturvedi and Ossakow, 1977; Kelley *et al.*, 1987).

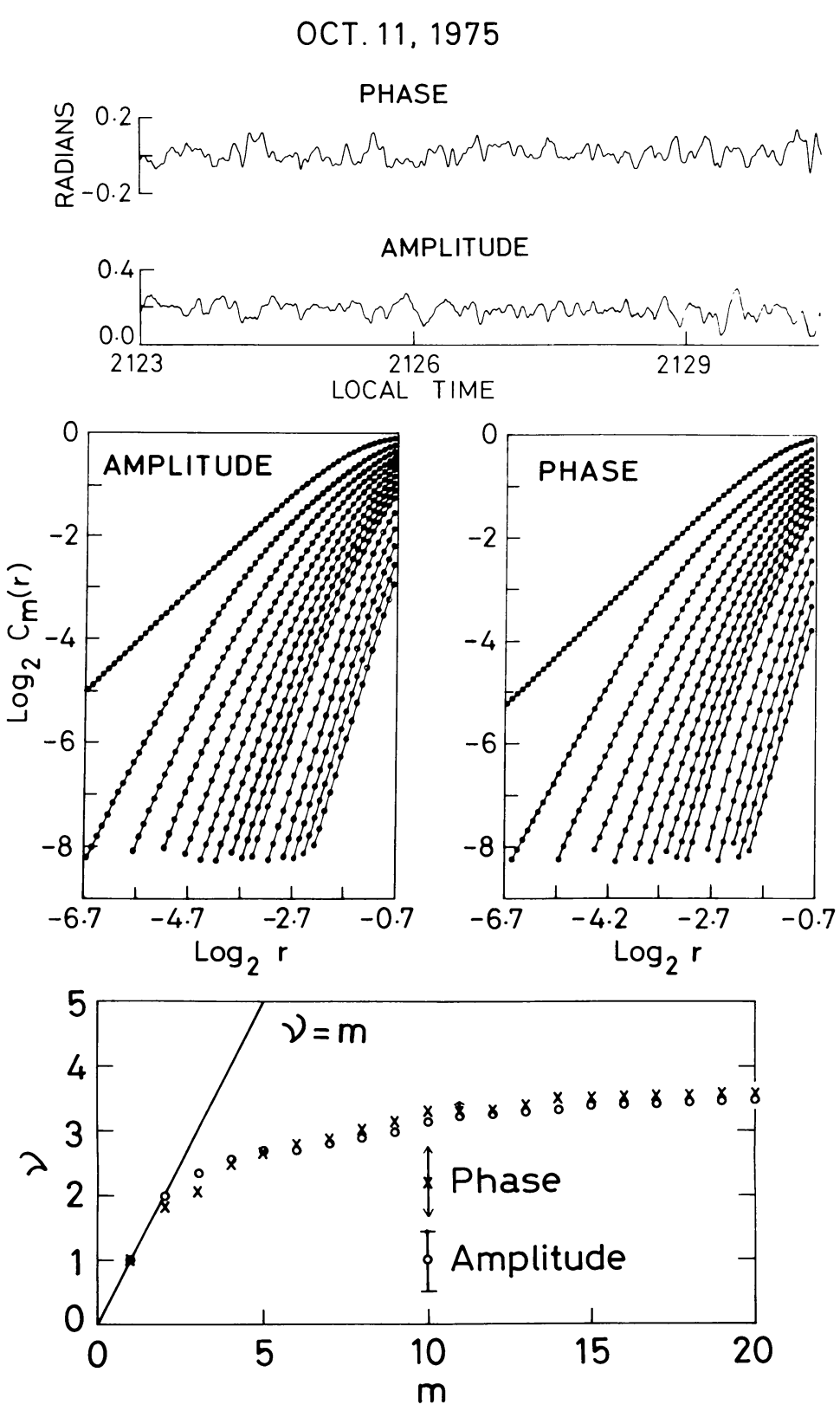


Fig. 18. (a) Filtered amplitude and phase scintillation data with $S_4 = 0.36$ and $\sigma_\phi = 0.21$ radians. (b) Plots of correlation integral $C_m(r)$ computed from the data for embedding dimension $m = 1$ to 10, 12, 14, 16, 18, and 20, starting from the left. (c) Slope $\nu$ in the linear range of plots in (b) as a function of $m$. Purely stochastic behavior would yield the straight line $\nu = m$. Here $\nu$ is seen to approach a constant value $D_2 \approx 3.4$ for sufficiently high values of $m$ for both amplitude and phase data, indicating low dimensionality for the ionospheric density fluctuations (Bhattacharyya, 1990).

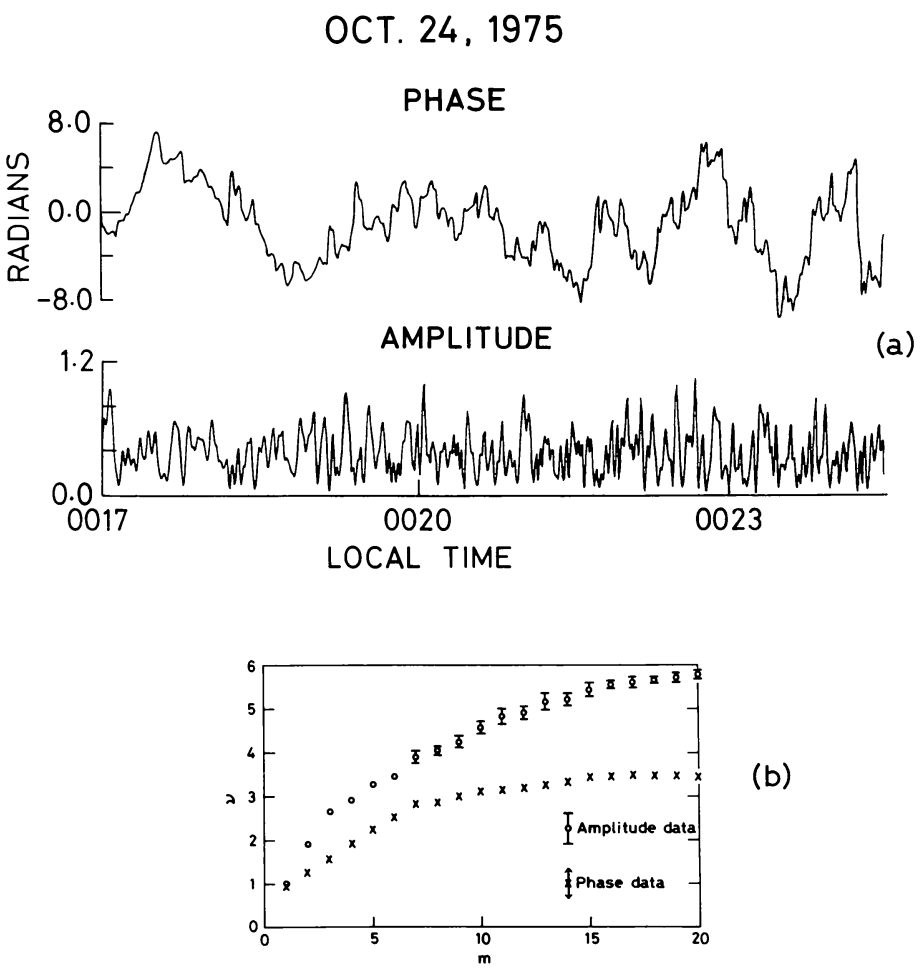


Fig. 19. (a) Same as Figure 18(a) for strong scintillations with $S_4 = 0.94$ and $\sigma_\phi = 3.35$ radians. (b) Same as Figure 18(c) for the data shown in Figure 19(a). The value of $D_2$ obtained for phase scintillations is substantially lower than that obtained for amplitude scintillations (Bhattacharyya, 1990).

(3) Effects on radio waves reflected from an ionosphere permeated by irregularities (Wagen and Yeh, 1989; Rand and Yeh, 1991).

(4) Scattering from a target in the presence of ionospheric irregularities (Yeh, 1983; Lure *et al.*, 1989; Knepp and Houpis, 1991).

In conclusion, it is seen that apart from the practical utility of scintillation studies in the context of their role in transionospheric communication links, there exist a number of geophysical problems where scintillation measurements can be utilized to provide useful inputs, through various parameters that can be computed from such observations.

## References

Aarons, J.: 1977, *IEEE Trans. Antennas Propagat.* **AP-25**, 729.

Aarons, J.: 1982, *Proc. IEEE* **70**, 360.

Barabenenkov, Yu. N., Kravstov, Yu. A., Rytov, S. M., and Tatarskii, V. I.: 1971, *Soviet Phys. Uspekhi* **13**, 551.

Basu, Su and Basu, S.: 1985, *J. Atmospheric Terrest. Phys.* **47**, 753.

Basu, Su and Kelley, M. C.: 1979, *Radio Sci.* **14**, 471.
Basu, S., Aarons, J., and Balsley, B. B.: 1977, *J. Geophys. Res.* **82**, 5262.
Basu, S., Basu, Su., Aarons, J., McClure, J. P., and Cousins, M. D.: 1978, *J. Geophys. Res.* **83**, 4219.
Basu, S., Basu, Su., LaBelle, J., Kudeki, E., Feier, B. G., Kelley, M. C., Whitney, H. E., and Bushby, A.: 1986, *J. Geophys. Res.* **91**, 5526.
Basu, S., Mackenzie, E., Basu, S., Carlson, H. C., Hardy, D. A., Rich, F. J., and Livingston, R. C.: 1983, *Radio Sci.* **18**, 1151.
Basu, S., McClure, J. P., Basu, Su., Hanson, W. B., and Aarons, J.: 1980, *J. Geophys. Res.* **85**, 5119.
Basu, Su., Basu, S., McClure, J. P., Hanson, W. B., and Whitney, H. E.: 1983, *J. Geophys. Res.* **88**, 403.
Basu, Su., Basu, S., Weber, E. J., and Coley, W. R.: 1988, *Radio Sci.* **23**, 545.
Basu, S., Basu, Su., Valladares, C. E., Dasgupta, A., and Whitney, H. E.: 1986, *J. Geophys. Res.* **91**, 270.
Basu, Su., Basu, S., Costa, E., Bryant, C., Valladares, C. E., and Livingston, R. C.: 1991, *Radio Sci.* **26**, 1079.
Berry, M. V.: 1977, *J. Phys.* **A10**, 2061.
Bhattacharyya, A.: 1990a, *Geophys. Res. Letters* **17**, 733.
Bhattacharyya, A.: 1990b, (preprint).
Bhattacharyya, A. and Rastogi, R. G.: 1986a, *J. Geophys. Res.* **91**, 11359.
Bhattacharyya, A. and Rastogi, R. G.: 1986b, *J. Atmospheric Terrest. Phys.* **48**, 463.
Bhattacharyya, A. and Rastogi, R. G.: 1991, *Radio Sci.* **26**, 439.
Bhattacharyya, A. and Yeh, K. C.: 1988, *Radio Sci.* **23**, 791.
Bhattacharyya, A., Franke, S. J., and Yeh, K. C.: 1989, *J. Geophys. Res.* **94**, 11959.
Bhattacharyya, A., Rastogi, R. G., and Yeh, K. C.: 1990, *Radio Sci.* **25**, 289.
Bhattacharyya, A. and Rastogi, R. G.: 1985, *Radio Sci.* **20**, 935.
Booker, H. G. and Majidi Ahi, G.: 1981, *J. Atmospheric Terrest. Phys.* **43**, 1199.
Booker, H. G., Ferguson, J. A., and Vats, H. O.: 1985, *J. Atmospheric Terrest. Phys.* **47**, 381.
Booker, H. G., Ratcliffe, J. A., and Shinn, D. H.: 1950, *Phil. Trans. Roy. Soc. London Ser.* **A242**, 579.
Bramley, E. N.: 1954, *Proc. Roy. Soc. London Ser* **A225**, 515.
Briggs, B. H.: 1975, *Cont. Phys.* **16**, 469.
Briggs, B. H., Phillips, G. F., and Shinn, D. H.: 1950, *Proc. Phys. Soc.* **B63**, 106.
Chaturvedi, P. K., and Kaw, P. K.: 1975, *Geophys. Res. Letters* **2**, 499.
Chaturvedi, P. K., and Ossakow, S. L.: 1977, *Geophys. Res. Letters* **4**, 558.
Costa, E. and Kelley, M. C.: 1978, *J. Geophys. Res.* **83**, 4359.
Costa, E., Fougere, P. F., and Basu, S.: 1988, *Radio Sci* **23**, 141.
Crane, R. K.: 1976, *J. Geophys. Res.* **81**, 2041.
Crane, R. K.: 1977, *Proc. IEEE* **65**, 180.
Davies, K., Donnelly, R. F., Grubb, R. N., Rama Rao, P. V. S., Rastogi, R. G., Deshpande, M. R., Chandra, H., Vats, H. O., and Sethia, G.: 1979, *Radio Sci.* **14**, 85.
Davies, K., Fritz, R. B., Grubb, R. N., and Jones, J. E.: 1975, *Radio Sci.* **10**, 785.
Dyson, P. L., McClure, J. P., and Hanson, W. B.: 1974, *J. Geophys. Res.* **79**, 1497.
Eckmann, J. P. and Ruelle, D.: 1985, *Rev. Mod. Phys.* **57**, 617.
Elkins, T. J. and Papagiannis, M. D.: 1969, *J. Geophys. Res.* **74**, 4105.
Fante, R. L.: 1976, *Radio Sci.* **11**, 215.
Farley, D. T., Ierkic, H. M., and Fejer, B. G.: 1981, *J. Geophys. Res.* **86**, 1467.
Fejer, B. G. and Kelley, M. C.: 1980, *Rev. Geophys. Space Phys.* **18**, 401.
Fejer, B. G., Kudeki, E., and Farley, D. T.: 1985, *J. Geophys. Res.* **90**, 12249.
Franke, S. J.: 1987, *Radio Sci.* **22**, 643.
Franke, S. J. and Liu, C. H.: 1983, *J. Geophys. Res.* **88**, 7075.
Franke, S. J. and Liu, C. H.: 1985, *Radio Sci.* **20**, 403.
Franke, S. J., Liu, C. H., and Fang, D. J.: 1984, *Radio Sci.* **19**, 695.
Fremouw, E. J., Leadbrand, R. L., Livingston, R. C., Cousins, M. D., Rino, C. L., Fair, B. C., and Long, R. A.: 1978, *Radio Sci.* **13**, 167.
Fremouw, E. J., Secan, J. A., and Lansinger, J. M.: 1985, *Radio Sci.* **20**, 923.
Fujita, M., Sinno, K., and Ogawa, T.: 1982, *J. Atmospheric Terrest. Phys.* **44**, 13.
Gochelashvily, K. S. and Shishov, V. I.: 1971, *Opt. Acta* **18**, 767.
Haerendel, G.: 1974, Tech. rep., Max-Planck Institut für Physik and Astrophysik, Garching, Germany.
Hassam, A. B., Hall, W., Huba, J. D., and Keskinen, M. J.: 1986, *J. Geophys. Res.* **91**, 13513.
Herman, J. R.: 1966, *Rev. Geophys.* **4**, 255.

Hewish, A.: 1951, *Proc. Roy. Soc. London Ser.* **A209**, 81.
Huba, J. D., Hassam, A. B., Schwartz, I. B., and Keskinen, M. J.: 1985, *Geophys. Res. Letters* **12**, 65.
Keller, J. B.: 1969, *J. Opt. Soc. Amer.* **59**, 1003.
Kelley, M. C., LaBelle, J., Kudeki, E., Fejer, B. G., Basu, S., Basu, Su., Baker, K. D., Hanuise, C., Argo, P., Woodman, R. F., Swartz, W. E., Farley, D. T., and Meriweather Jr., J. W.: 1986, *J. Geophys. Res.* **91**, 5487.
Kelley, M. C., Livingston, R. C., Rino, C. L., and Tsunoda, R. T.: 1982, *J. Geophys. Res.* **87**, 5217.
Kelley, M. C., Seyler, C. E., and Zargham, S.: 1987, *J. Geophys. Res.* **92**, 10089.
Knepp, D. L. and Houpis, H. L. F.: 1991, *IEEE Trans.* **AP39**, 528.
Kudeki, E. and Franke, S. J.: 1986, *Geophys. Res. Letters* **13**, 1117.
Kudeki, E., Farley, D. T., and Fejer, B. G.: 1982, *Geophys. Res. Letters* **9**, 684.
Kumagai, H.: 1987, *Radio Sci.* **22**, 439.
Kumagai, H. and Ogawa, T.: 1986, *J. Atmospheric Terrest. Phys.* **48**, 221.
Kumagai, H., Hori, T., Ohbu, K., Isobe, T., Ouchi, E., Nishino, T., Ouchi, C., and Ogawa, T.: 1982, *J. Radio Res. Labs Japan* **29**, 151.
LaBelle, J. and Kelley, M. C.: 1986, *J. Geophys. Res.* **91**, 5504.
Lee, L. C.: 1974, *J. Math. Phys.* **15**, 1431.
Leitinger, R., Hartmann, G. K., Degenhardt, W., Hedberg, A., and Tanskanen, P.: 1982, *J. Atmospheric Terrest. Phys.* **44**, 369.
Liu, C. H. and Yeh, K. C.: 1977, *J. Atmospheric Terrest. Phys.* **39**, 149.
Liu, C. H., Wernik, A. W., Yeh, K. C., and Youakim, M. Y.: 1974, *Radio Sci.* **9**, 599.
Livingston, R. C., Rino, C. L., McClure, J. P., and Hanson, W. B.: 1981, *J. Geophys. Res.* **86**, 2421.
Lure, Y. M., Yang, C. C., and Yeh, K. C.: 1989, *Radio Sci.* **24**, 147.
Marians, M.: 1975, *Radio Sci.* **10**, 115.
Mercier, R. P.: 1962, *Proc. Cambr. Phil. Soc.* **58**, 382.
Mitra, S. N.: 1949, *Proc. Inst. Electr. Eng.* **96**, 441.
Moorcroft, D. R. and Arima, K. S.: 1972, *J. Atmospheric Terrest. Phys.* **34**, 437.
Muldrew, D. B. and Vickrey, J. F.: 1982, *J. Geophys. Res.* **87**, 8263.
Mullen, J. P., Whitney, H. E., Basu, S., Bushby, A., Lanat, J., and Pantoja, J.: 1977, *J. Atmospheric Terrest. Phys.* **39**, 1243.
Myers, W. J., Gjeldum, R. J., Liu, C. H., and Yeh, K. C.: 1979, *J. Geophys. Res.* **84**, 2039.
Ogawa, T., Sinno, K., Fujita, M., and Awaka, J.: 1980, *J. Atmospheric Terrest. Phys.* **42**, 637.
Rand, T. W., and Yeh, K. C.: 1990, *Radio Sci.* **26**, 1.
Ratcliffe, J. A.: 1956, *Rep. Progr. Phys.* **19**, 188.
Rino, C. L.: 1979a, *Radio Sci.* **14**, 1135.
Rino, C. L.: 1979b, *Radio Sci.* **14**, 1147.
Rino, C. L., Livingston, R. C., and Matthews, S. J.: 1978, *Geophys. Res. Letters* **5**, 1039.
Rino, C. L., Tsunoda, R. T., Petriceks, J., Livingston, R. C., Kelley, M. C., and Baker, K. D.: 1981, *J. Geophys. Res.* **86**, 2411.
Rino, C. L. and Livingston, R. C.: 1982, *Radio Sci.* **17**, 845.
Rino, C. L. and Owen, J.: 1980, *J. Geophys. Res.* **85**, 2941.
Rino, C. L. and Owen, J.: 1982, *Radio Sci.* **17**, 675.
Rufenach, C. L.: 1972, *J. Geophys. Res.* **77**, 4761.
Rumsey, V. H.: 1975, *Radio Sci.* **10**, 107.
Shishov, V. I.: 1974, *Radio Phys. Quantum Electron.* **17**, 1287.
Shkarofsky, I. P.: 1968, *Can. J. Phys.* **46**, 2133.
Singh, M., and Szuszczewicz, E. P.: 1984, *J. Geophys. Res.* **89**, 2313.
Singleton, D. G.: 1974, *J. Atmospheric Terrest. Phys.* **36**, 113.
Spatz, D. E., Franke, S. J., and Yeh, K. C.: 1988, *Radio Sci.* **23**, 347.
Tatarskii, V. I.: 1971, Nat. Tech. Inform. Service, Springfield, VA, U.S.A.
Umeki, R., Liu, C. H., and Yeh, K. C.: 1977a, *J. Geophys. Res.* **82**, 2752.
Umeki, R., Liu, C. H., and Yeh, K. C.: 1977b, *Radio Sci.* **12**, 311.
Uscinski, B. J. and Macaskill, C.: 1983, *J. Atmospheric Terrest. Phys.* **45**, 595.
Vacchione, J. D., Franke, S. J., and Yeh, K. C.: 1987, *Radio Sci.* **22**, 745.
Wagen, J.-F., and Yeh, K. C.: 1989, *Radio Sci.* **24**, 209.

Weber, E. J., Tsunoda, R. T., Buchau, J., Sheehan, R. E., Strickland, D. J., Whiting, W., and Moore, J. G.: 1985, *J. Geophys. Res.* **90**, 6497.
Wernik, A. W., Liu, C. H., and Yeh, K. C.: 1983, *Radio Sci.* **18**, 743.
Wernik, A. W., Liu, C. H., Franke, S. J., and Yeh, K. C.: 1990, *Radio Sci.* **25**, 883.
Yeh, K. C.: 1983, *Radio Sci.* **18**, 159.
Yeh, K. C. and Liu, C. H.: 1982, *Proc. IEEE* **70**, 324.
Yeh, K. C., Liu, C. H., and Youakim, M. Y.: 1975, *Radio Sci.* **10**, 97.
Zargham, S. and Seyler, C. E.: 1987, *J. Geophys. Res.* **92**, 10073.